Department of Applied Physics

Towards realistic orbit-following simulations of fast ions in ITER

Antti Snicker

Aalto University

DOCTORAL DISSERTATIONS

Aalto University publication series
DOCTORAL DISSERTATIONS 199/2014

Towards realistic orbit-following simulations of fast ions in ITER

Antti Snicker

A doctoral dissertation completed for the degree of Doctor of Science (Technology) to be defended, with the permission of the Aalto University School of Science, at a public examination held at the lecture hall K216 of the school on 9 December 2014 at 14.

Aalto University
School of Science
Department of Applied Physics
Fusion and Plasma Physics

Supervising professor
Mathias Groth

Thesis advisor
Taina Kurki-Suonio

Preliminary examiners
Dr. Toshihiro Oikawa, ITER Organization, France
Prof. Torbjörn Hellsten, KTH, Sweden

Opponent
Dr. Rob Akers, United Kingdom Atomic Authority, UK

Aalto University publication series
DOCTORAL DISSERTATIONS 199/2014

ISBN 978-952-60-5993-8 (printed)
ISBN 978-952-60-5994-5 (pdf)
ISSN-L 1799-4934
ISSN 1799-4934 (printed)
ISSN 1799-4942 (pdf)
http://urn.fi/URN:ISBN:978-952-60-5994-5

Images: Antti Snicker, Jyrki Hokkanen (CSC)

Unigrafia Oy
Helsinki 2014

Finland

Publication orders (printed book):
antti.snicker@aalto.fi

441 697
Printed matter

Aalto University

Abstract

Aalto University, P.O. Box 11000, FI-00076 Aalto www.aalto.fi

Author
Antti Snicker

Name of the doctoral dissertation
Towards realistic orbit-following simulations of fast ions in ITER

Publisher School of Science

Unit Department of Applied Physics

Series Aalto University publication series DOCTORAL DISSERTATIONS 199/2014

Field of research Fusion science

Manuscript submitted 22 September 2014 **Date of the defence** 9 December 2014

Permission to publish granted (date) 17 November 2014 **Language** English

☐ **Monograph** ☒ **Article dissertation (summary + original articles)**

Abstract

One of the main scientific goals of the international ITER experiment is to provide understanding of burning plasmas, including the behavior of fusion-born alpha particles. These particles form both a potential risk for the first wall and a massive source of free energy in the plasma. Such free energy can drive a multitude of MHD modes, most notably the Alfvénic ones, that can lead to increased transport and even losses of fast ions.

In this work, the alpha particle physics has been studied using kinetic orbit-following Monte Carlo code ASCOT. The code was enhanced with two new physics models. The first model relaxes the usual guiding center (GC) approximation used to save computation time. In some cases, this approximation is not valid and the full gyro motion (FO) has to be resolved. The second model is for fast ion relevant MHD modes and its implementation allows taking into account electromagnetic fields due to these modes.

When the MHD model was used to simulate ITER plasmas, the wall power loads due to fast particles were not found to exceed the design limits of the wall materials even for unrealistically large perturbations. However, redistribution of fast ions was observed to alter the alpha particle heating profile and neutral beam ion (NBI) driven current profile.

Fusion alphas were simulated for the ITER 15 MA scenario using different integration methods. Following the full gyro motion gave slightly larger alpha particle wall power loads than the GC method. Since the FO method uses more than 50 times more CPU than GC integration, a third method was introduced as a compromise between the speed and accuracy: the GC method is used in the plasma core and FO integration is activated in the vicinity of the wall.

Finally, alpha-driven current and torque in ITER were studied using different magnetic field configurations. It was found that, independent of the magnetic configurations, the alpha-driven current is less than 1% of the total plasma current for both 9 MA and 15 MA baseline scenarios. On the contrary, the alpha-driven torque depends on the magnetic field configuration. While in the axisymmetric case the total torque was found to be close to zero, with realistic 3D effects the alpha particles produced substantial torque, about one tenth of that driven by the NBI particles, but in direction opposite to it.

Keywords alpha particles, plasma, ITER, ASCOT, guiding center

ISBN (printed) 978-952-60-5993-8 **ISBN (pdf)** 978-952-60-5994-5

ISSN-L 1799-4934 **ISSN (printed)** 1799-4934 **ISSN (pdf)** 1799-4942

Location of publisher Helsinki **Location of printing** Espoo **Year** 2014

Pages 149 **urn** http://urn.fi/URN:ISBN:978-952-60-5994-5

A? Aalto-yliopisto

Tiivistelmä

Aalto-yliopisto, PL 11000, 00076 Aalto www.aalto.fi

Tekijä
Antti Snicker

Väitöskirjan nimi
Towards realistic orbit-following simulations of fast ions in ITER

Julkaisija Perustieteiden korkeakoulu

Yksikkö Department of Applied Physics

Sarja Aalto University publication series DOCTORAL DISSERTATIONS 199/2014

Tutkimusala Fusion science

Käsikirjoituksen pvm 22.09.2014 **Väitöspäivä** 09.12.2014

Julkaisuluvan myöntämispäivä 17.11.2014 **Kieli** Englanti

☐ **Monografia** ☒ **Yhdistelmäväitöskirja (yhteenveto-osa + erillisartikkelit)**

Tiivistelmä

Maailman ensimmäisessä fuusioreaktorissa, ITERissä, on tarkoitus oppia ymmärtämään palavien plasmojen fysiikkaa ja siten valmistella tietä kaupalliselle fuusioenergialle. Fuusioreaktioissa syntyvät nopeat alfahiukkaset sekä neutraalisuihkukuumennuksesta (NBI) syntyneet nopeat ionit aiheuttavat riskin ensiseinämän kestävyydelle. Hiukkasten sisältämä vapaa energia mahdollistaa monenlaiset magnetohydrodynaamiset (MHD) epästabilisuudet. Nämä MHD-häiriöt voivat aiheuttaa nopeiden hiukkasten kulkeutumista jopa ulos plasmasta.

Tässä työssä on tutkittu alfa- ja NBI-hiukkasten fysiikkaa käyttäen apuna kineettistä Monte-Carlo menetelmään perustuvaa radanseurantaohjelmistoa nimeltään ASCOT. Koodia on täydennetty numeerisilla malleilla, joista ensimmäinen mahdollistaa johtokeskusmenetelmän (GC) testaamisen ja tarvittaessa korvaa sen. Menetelmässä ratkaistaan hiukkasen gyroliike magneettikentän ympäri (FO). Toinen malli ottaa huomioon tiettyihin MHD ilmiöihin liittyvien sähkömagneettisten häiriöiden vaikutuksen nopeisiin hiukkasiin.

Ensimmäistä mallia sovellettiin ITER:n perusplasmalle (15 MA) ja havaittiin, että FO menetelmällä laskettu alfahiukkasten aiheuttama seinäkuorma on suurempi kuin käytettäessä GC menetelmää. Koska FO menetelmä vaati noin 50 kertaa enemmän laskenta-aikaa, esiteltiin uusi hybridimenetelmä, joka siirtyy käyttämään FO radanseurantaa vain seinämien lähistöllä.

MHD-mallia käytettiin useissa erilaisissa ITER-simuloinneissa. MHD-häiriöt eivät aiheuttaneet missään tapauksessa merkittävää lisäystä nopeiden hiukkasten tuottamiin seinäkuormiin. Sen sijaan MHD-häiriöt vaikuttavat nopeiden hiukkasten jakaumaan plasman sisällä. Tämä uudelleen jakautuminen aiheutti muutoksia sekä alfahiukkasten kuumennusprofiilissa että NBI-hiukkasten ajamassa virtaprofiilissa.

Työssä laskettiin myös alfahiukkasten aiheuttama sähkövirta ja vääntömomentti erilaisten magneettikentän häiriöiden läsnäollessa. Alfahiukkasten synnyttämä virta oli kaikissa tapauksissa alle 1% kokonaisplasmavirrasta. Alfahiukkasten ajaman väännön puolestaan havaittiin riippuvan ulkoisista häiriöistä: aksiaalisesti symmetrisessä tapauksessa väännön komponentit summautuivat nollaan, mutta 3D häiriöiden läsnäollessa alfavääntö oli nollasta poikkeava. Alfaväännön suuruus on kuitenkin kertaluokkaa pienempi kuin NBI-hiukkasten aiheuttama vääntö ja lisäksi vastakkaissuuntainen.

Avainsanat alpha particles, plasma, ITER, ASCOT, guiding center

ISBN (painettu) 978-952-60-5993-8	**ISBN (pdf)** 978-952-60-5994-5	
ISSN-L 1799-4934	**ISSN (painettu)** 1799-4934	**ISSN (pdf)** 1799-4942
Julkaisupaikka Helsinki	**Painopaikka** Espoo	**Vuosi** 2014
Sivumäärä 149	**urn** http://urn.fi/URN:ISBN:978-952-60-5994-5	

Preface

This work has been carried out at the Fusion and Plasma physics group of Aalto University during 2010-2014. Without the financial support from Professors Rainer Salomaa, Mathias Groth and Taina Kurki-Suonio, this thesis would have not seen the daylight. The work that I have done have also received funding from the Academy of Finland, Eemil Aaltonen Foundation, and Finnish Foundation for Technology promotion.

From Taina, the financial support is only a minor fraction of the help that I have received during these years. I genuinely think that the spirit in our ASCOT group is one of a kind - it has been a pleasure to work here. Hence, it is the whole group of Eero (ex-ASCOT), Otto, Simppa, Seppo, Juho (+summer students) that I am grateful for.

Life cannot, unfortunately, be all joy. In those days when I have needed motivation and help to get through tougher times, my wife Eeva has always been there for me. Every person needs a bedrock to build one's life on, and Eeva is mine. My hobbies have always balanced the busy and tiring office work. Particularly, I would like to thank my friends Juha and Erno for all the good times.

As far as I know, I will be the first PhD in our family. That would not have been possible without the encouragement from my parents, thank you for that.

Espoo, November 18, 2014,

Antti Snicker

Contents

Preface **1**

Contents **3**

List of Publications **5**

Author's Contribution **7**

1. Introduction **9**

1.1 Fusion as energy source 9

1.2 From fusion reactions to reactors 10

1.3 Reactor relevant fast particle physics 12

1.4 Introduction into kinetic fast ion orbit-following theory and simulations 13

1.5 Content of this thesis 14

1.6 Organization of the thesis 16

2. Numerical tools - the ASCOT code **17**

2.1 Background for the simulation model 17

2.1.1 The tokamak 17

2.1.2 Coordinate systems for a tokamak 18

2.2 Simulation model of the ASCOT code 20

2.2.1 Equations of motion 21

2.2.2 Coulomb interactions and wall collision model 23

2.2.3 Running ASCOT on a (super)computer 25

3. Development of numerical models **27**

3.1 Full orbit particle tracing 27

3.2 Magnetohydrodynamical instabilities 31

4. Results of numerical simulations **35**

4.1 ITER wall power loads with full orbit tracing 35
4.2 Alpha particle current and torque drive in ITER 38
4.3 Benchmarking, verification and validation of the MHD model in ASCOT 43
4.4 The effect of NTMs and TAEs on fast ions in ITER 49

5. Summary, discussion and outlook **55**
5.1 Summary and discussion 55
5.2 Outlook 56

Bibliography **59**

Publications **69**

List of Publications

This thesis consists of an overview and of the following publications which are referred to in the text by their Roman numerals.

I A. Snicker, S. Sipilä and T. Kurki-Suonio. Realistic simulations of fast-ion wall distribution including effects due to finite Larmor radius. *IEEE Transactions on Plasma Science*, **38, pp. 2177-2184**, 2010.

II A. Snicker, T. Kurki-Suonio and S. Sipilä. Orbit-following fusion alpha wall load simulation for ITER scenario 4 including full orbit effects. *Nuclear Fusion*, **52, 094011**, 2012.

III A. Snicker, E. Hirvijoki and T. Kurki-Suonio. Power loads to ITER first wall structures due to fusion alphas in non-axisymmetric magnetic field including the presence of MHD modes. *Nuclear Fusion*, **53, 093028**, 2013.

IV E. Hirvijoki, A. Snicker, T. Korpilo, P. Lauber, E. Poli, M. Schneller and T. Kurki-Suonio. Alfvén eigenmodes and neoclassical tearing modes for orbit-following implementations. *Computer physics communications*, **183, pp. 2589-2593**, 2012.

V A. Snicker, O. Asunta, H. Ylitie, T. Kurki-Suonio, M. Schneider and S. Pinches. Alpha particle current drive and rotation in ITER baseline scenarios with 3D perturbations. *Nuclear Fusion*, submitted to NF, 2014.

VI T. Kurki-Suonio, O. Asunta, T. Koskela, A. Snicker. T. Hauff, F. Jenko, E. Poli and S. Sipilä. Fast ion power loads in ITER first wall structures in the presence of NTMs and microturbulence. *Nuclear Fusion*, **51, 083041**, 2011.

Author's Contribution

Publication I: "Realistic simulations of fast-ion wall distribution including effects due to finite Larmor radius"

The author was the main developer of numerical tools presented in this publication. Author also was responsible for the writing part.

Publication II: "Orbit-following fusion alpha wall load simulation for ITER scenario 4 including full orbit effects"

The author was responsible for the analysis of numerical results presented in the publication. Author was also responsible for the manuscript.

Publication III: "Power loads to ITER first wall structures due to fusion alphas in non-axisymmetric magnetic field including the presence of MHD modes"

The author was responsible of numerical simulations, numerical analysis and also the writing of the manuscript.

Publication IV: "Alfvén eigenmodes and neoclassical tearing modes for orbit-following implementations"

The author provided background information for the main author of this publication and also contributed to the writing of the publication. The implementation of the model was carried out in co-operation with the main author.

Publication V: "Alpha particle current drive and rotation in ITER baseline scenarios with 3D perturbations"

The author did most of ASCOT simulations, gathered simulation results, analyzed them and wrote the article with the help of comments by co-authors.

Publication VI: "Fast ion power loads in ITER first wall structures in the presence of NTMs and microturbulence"

The author was responsible of numerical simulations for NTMs and also contributed on writing of corresponding parts of the manuscript.

1. Introduction

1.1 Fusion as energy source

Rapidly increasing demand for a clean and safe energy combined with the increasing energy consumption per person [1] poses an serious issue for mankind. All stones should be turned in order to solve this global problem. Thermonuclear fusion, using deuterium (D) and tritium (T) as a fuel and a tokamak design for the reactor, is one of the most promising solutions to the above mentioned problem. It may, however, turn out that fusion will not solve the energy problem but potentially it can cover a major fraction of the needed energy with a clean and safe solution. In any case, fusion is simply too big stone not to look underneath.

Mankind – literally, countries covering more than a half of the world's population are involved – has unified its know-how and economical forces to build and operate the experimental thermonuclear fusion reactor ITER – a tokamak currently been build in Cadarache, France [2]. So far, the scientific feasibility of nuclear fusion is considered to be on a solid basis whereas the main objective of ITER is to assess the technological feasibility. The work towards commercial fusion does not, however, end at the ITER project. At the same time as ITER is proving the technological feasibility for nuclear fusion, the DEMO reactor will be introduced [3]. The objective of DEMO is to prove the economical feasibility of nuclear fusion, i.e. to show that the price of the electricity produced in the fusion power plant can compete with other energy production methods in the future.

1.2 From fusion reactions to reactors

Even though there are no fusion reactors available on Earth, already today basically all the electricity produced on Earth, omitting fission energy, can be backtracked to fusion reactions in the Sun. These reactions provide the radiation that is used by, e.g., solar cells and by all hydro power plants.

Mimicking the Sun on Earth is, unfortunately, extremely challenging. In the Sun, fusion is taking place with a rather complicated chain of reactions summing up to

$$4 \cdot {}^1\mathrm{H} + 2 \cdot e^- \longrightarrow {}^4\mathrm{He} + 6 \cdot \gamma + 2 \cdot \nu_e, \tag{1.1}$$

where e^- is an electron, γ is a photon and ν_e is an electron neutrino. The conditions in the core of the Sun, where these reactions take place, cannot be reached on Earth. Consequently, other fusion reactions have to be considered to enable fusion on Earth.

The first requirement is that the fusion reaction has to have high enough cross-section, i.e. sufficiently high probability for it to happen at achievable temperatures. More stringent requirement is brought in by the so-called Lawson criterion [4] for plasma to ignite, i.e. to keep the fusion conditions without an auxiliary power input. The simplified Lawson criterion reads

$$nT\tau_E \leq \frac{12 k_B T^2}{E_F \langle \sigma v \rangle}, \tag{1.2}$$

where n is the density, T the temperature, $\langle \sigma v \rangle$ the fusion reaction rate, τ_E the energy confinement time and E_F the energy of the charged fusion product responsible for maintaining the fusion-relevant temperatures (neutrons will escape the magnetically confined plasma). This criterion suggests that when the tripple product of $nT\tau_E$ increases above a temperature dependent threshold value, the plasma ignites.

According to figure 1.1, the most convenient reaction to enable fusion on Earth is the one with deuterium and tritium fusing to helium:

$${}^2\mathrm{H} + {}^3\mathrm{H} = \mathrm{D} + \mathrm{T} \longrightarrow {}^4\mathrm{He}\ (3.5\ \mathrm{MeV}) + n\ (16.1\ \mathrm{MeV}). \tag{1.3}$$

This reaction has the minimum of the Lawson criterion at the lowest temperature of around 14 keV, and also the value of the tripple product is several magnitudes lower than with the competing reactions. For the DT reaction, $n\tau_E$ needs to be around $2 \cdot 10^{14}$ cm^{-3}s at the temperature of 15 keV to ignite the plasma.

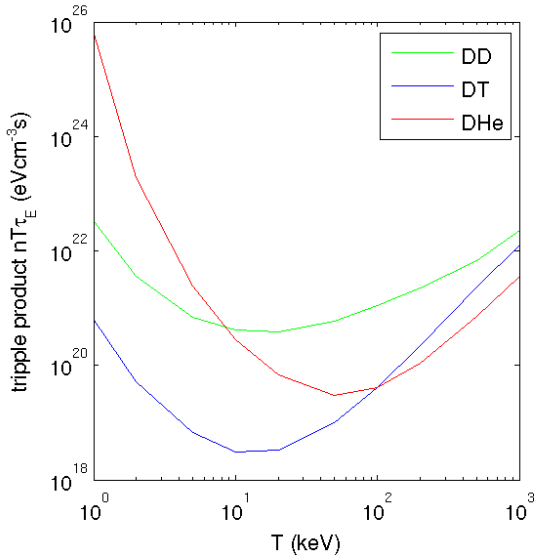

Figure 1.1. The fusion tripple product as a function of the temperature showing the Lawson criterion for fusion for DD, DT and DHe fusion reactions. According to the figure, DT provides the best conditions to obtain fusion on Earth. The data for cross sections is from [5].

Deuterium is found from the sea water and will not cause problems for neither the adundancy nor the equal distribution among the mankind. Tritium, on the other hand, is more complicated case, being a radioactive isotope with a half-life of 12 years. The strategy is to breed tritium inside the reactor from lithium with the breeding reactions

$$n + {}^6\mathrm{Li} \longrightarrow \mathrm{T} + {}^4\mathrm{He} + \ (4.8\ \mathrm{MeV}) \tag{1.4}$$

$$n + {}^7\mathrm{Li} \longrightarrow \mathrm{T} + {}^4\mathrm{He} + n - \ (2.5\ \mathrm{MeV}). \tag{1.5}$$

Hence, for the tritium breeding both neutrons with suitable energy and lithium are needed. A neutron is already generated by every DT reaction but the number of neutrons is sufficient only after multiplication reactions as some of the neutrons do not undergo the breeding reaction. Moreover, the energy of the neutrons, without a moderator to slow them down, is too high for optimal tritium breeding. Lithium is abundant in the soil, and also very equally distributed world wide.

The tokamak reactor fuel concept can be summarized as follows: The fuel transported to the power plant consists of deuterium and lithium. In the reactor core, the fuel consists of deuterium and tritium. On the first wall, there will be a blanket containing lithium for the tritium breeding. The blanket also contains circulating water, or other fluid, to both

slow the 16 MeV neutrons down to energies where the tritium breeding is maximized and to convert the fusion energy to heat in the water. Eventually, the pressurized hot water is used like in the traditional power plants to generate electricity, i.e. it is first steamed and then led to turbines.

1.3 Reactor relevant fast particle physics

Fusion using deuterium and tritium was selected as the most promising option. However, this reaction leads to activation of wall materials by high-energy neutrons. Therefore, the DT reaction is replaced by the DD mock-up reaction as the basic fusion research.

One of the most important features of DT physics, not present in DD mock-up plasmas, is the vast number of fusion-born alphas present in DT plasmas. These particles have a crucial role in ensuring a sufficiently high temperature in the plasma. Alpha particles are born with a 3.5 MeV energy and are expected to transfer the majority of their energy to the plasma fuel. In a burning plasma, this energy is sufficient to ensure self-sustained heating of the plasma [4, 6].

The transport of these alpha particles must be understood in the realistic burning plasma conditions. If this is not the case, not only is part of the alpha power lost but, even worse, these high-energy particles may lead to serious damage of the first wall. Furthermore, these alpha particles provide free energy source in the plasma. It has been shown [7] that this free energy can excite several magnetohydrodynamical (MHD) instabilities. The situation is even more complicated as the MHD instabilities act back to alpha particles potentially redistributing them or leading them to orbits that intersect with the first wall (lost orbits) [8, 9].

Predicting the fusion alpha behaviour in burning plasma is, thus, very important for successful operation of ITER. Computer simulations are a way to obtain such predictions without unrealistic assumptions such as very simplistic magnetic field or absence of MHD modes and limiting material surfaces. In order to be reliable, these computer simulations need to be validated using the experimental data from existing experiments. In addition to fusion alphas, also 1 MeV deuterons from NBI heating pose similar problems and have to be understood. These fast particles are the topic of this thesis.

1.4 Introduction into kinetic fast ion orbit-following theory and simulations

One method to understand fast ion behaviour in tokamaks is to numerically solve the kinetic equation of these particles. As a solution of this equation, the distribution function, i.e. the probability of finding fast particles at the given phase-space location, is obtained. This function contains all essential information about the fast particles.

The first step towards the modern simulations was the application of a so-called guiding center approximation, where the fast gyration of the particles around the magnetic field line was replaced by the movement of the particles' guiding center. This work was initiated by the father of the plasma physics, Hannes Alfvén, who discovered in his paper from 1940 [10] that the magnetic moment $\mu = \frac{mv_\perp^2}{2B}$ is an adiabatic invariant, and that this invariant is associated with the particle motion around the magnetic field line. This result is essential for the later work with the guiding center theory. Alfvén also derived the guiding center equations of motion by averaging over the fast gyration and his results were later on reviewed by Northrup [11].

Later on, it was noticed that the Hamiltonian nature of the system was broken in the averaging procedure. This had dramatic consequences: e.g. the total energy of the particle was not conserved. The problem was solved in early 1980s, mainly by Littlejohn [12–14]. In his treatment of the non-canonical Hamiltonian guiding center theory, the obvious increment was to carry the guiding center approximation in such a way that the Hamiltonian nature of the system was conserved. This work was reviewed by Cary and Brizard [15]. This review can be considered as the basis for the modern guiding center particle tracing applications.

Along the development of the guiding center tracing, the transport processes in a hot plasma were considered [16]. To zeroth order, it is appropriate to assume that the Hamiltonian motion dominates the transport of fast particles. However, when the particles are followed long enough, compared to the slowing-down time of the particles, the collisions between the fast ions and the thermal background plasma become equally important. As a result, neoclassical transport of the traced particles is solved.

Already in the 1980s, the interaction of the fast ions with electromagnetic waves was realized to affect the fast ion transport and, thereby, the kinetic equation of fast particles [17]. In burning plasmas, these interac-

tions seem to play a key role and, therefore, the research for this wave-particle interaction has recently been the topic for several studies.

It is known that microturbulence is the main reason for the increased transport of the bulk plasma. However, microturbulent transport of fast ions [18] is shown, in Publication VI, to be of the order of the statistical error in the simulations. Therefore, it is justified to omit turbulent transport from the fast ion simulations.

In 1990s, it was realized that the shape of the magnetic field has a clear effect on the solution of the kinetic equation of fast particles [19, 20]. At first stage, realistic 2D models were created to take into account the shape of the tokamak plasmas. As a result, analytical magnetic field models were replaced by tabulated data. In 2000s, the 3D geometry of the magnetic field was found to further affect the fast ions leading to additional transport processes, and thereby, changed the solution of the kinetic equation of fast particles [21–23].

1.5 Content of this thesis

The coupling of the different transport processes were, hence, not done in the most general way. The guiding center approximation was often used, even though in some cases the guiding center approximation is not valid. The simplest example being a case of strongly changing magnetic field within the gyration radius of the fast particle. The natural solution for this case is to follow the actual particle instead of its guiding center.

Having a tool with options to both follow guiding centers and full orbits is beneficial as the validity of the guiding center approximation can always be checked. Therefore, the option to trace full orbits was implemented and applied using the ASCOT code [24]. While the full orbit following has already been considered by various codes, e.g., GOURDON, SPIRAL [25], and LOCUST [26, 27], these codes do not have the capability to follow guiding centers. Investigations of full orbit fast particle motion versus guiding center approximation is described in the first half of the thesis.

The standard guiding center formalism can not explain the interactions of fast particles with the various MHD modes that are routinely observed in various experimental devices [28, 29]. The modes are accompanied with a perturbation in the electromagnetic fields that affect the particle motion. The motion due to these perturbations compete with the

Hamiltonian motion assuming MHD quiescent plasma, e.g. when there are many modes overlapping with each other or when strong enough single mode appears. Therefore, accurate guiding center simulations should take these perturbations into account.

There were a few dedicated codes to investigate wave-particle interactions, such as HAGIS [30] and ORBIT [17]. However, the effects of the 3D magnetic field perturbations due to TF ripple, TBMs or ELM mitigation coils were neglected, without a necessity, in these codes. To this end, the second half of this thesis is dedicated to inclusion of MHD modes in ASCOT code, where 3D magnetic field is inherently present together with several other 3D effects like the first wall as illustrated in figure 1.2. This model, coupling the 3D neoclassical transport with the wave-particle interaction, is presented and applied in this thesis for ITER plasmas.

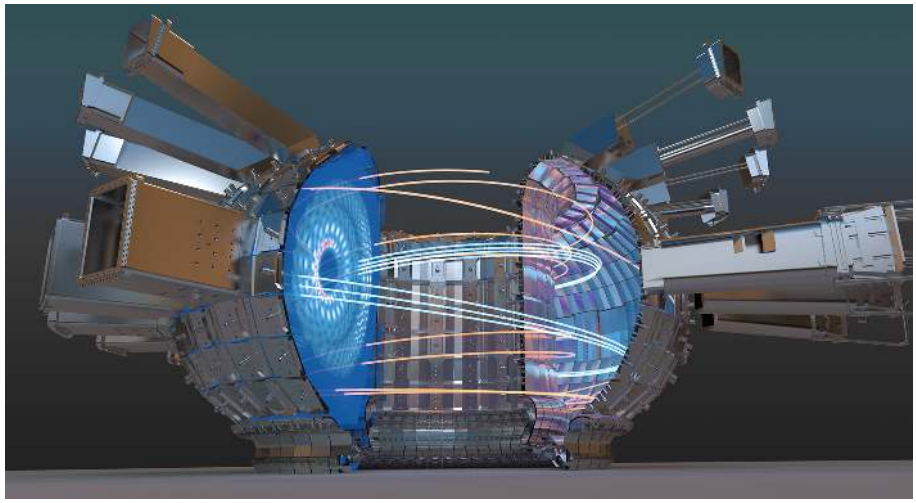

Figure 1.2. An artistic view of the fast ion orbits (red and blue lines) in the magnetic field containing Alfvénic perturbation. The magnetic field perturbation due to Alfvénic mode is shown in the left cross-section. Full 3D design for both the magnetic field and the wall of ITER tokamak are used. © Jyrki Hokkanen, CSC.

For the simulations, two ITER baseline scenarios are considered. An inductive scenario with Q=10, where Q stands for fusion gain defined by the ratio of the thermonuclear power to the external heating power applied, and 15 MA plasma current was selected as the main ITER project mission to study the technological feasibility of the thermonuclear fusion. Steady-state scenario with Q=5 and 9 MA plasma current was selected as it is the primary aim for ITER and, at the moment, the best candidate for the fusion power plant operation.

1.6 Organization of the thesis

This thesis is organized as follows. After the introduction presented above, the most important tool used in the thesis, the ASCOT suite of codes, is presented in chapter 2. Only the key aspects related to this thesis are discussed. In the chapter 3, the numerical development within the context of this thesis is summarized. The energy conservation properties missing from the papers attached to the thesis, are presented here. The results of numerical simulations are summarized in the chapter 4. In each section of this chapter, a separate physics study is described. The whole thesis is discussed, summarized, and an outlook is presented in the chapter 5. After the compilation part of the thesis, the publications are attached.

2. Numerical tools - the ASCOT code

This chapter presents the numerical tool to solve the kinetic equation of fast ions in tokamaks. As an introduction, the tokamak environment and the coordinate systems to be used later on in the thesis will be presented.

2.1 Background for the simulation model

2.1.1 The tokamak

The tokamak is the leading branch to obtain the burning plasma conditions. The main competitors are stellarators like Wendelstein 7X [31] and laser ignited fusion experiments like NIF [32]. Tokamaks and stellarators belong to the magnetically confinement fusion experiments while the plasma in a laser fusion experiment is confined only by the inertia of the plasma particles. Only tokamaks are considered within this thesis.

The tokamak principle is to maximize the energy confinement time to ignite the plasma. Sufficient energy confinement is obtained by large and properly oriented magnetic fields that keep the charged plasma particles inside the vessel walls. The main component of the magnetic field is toroidal and it is generated by poloidally oriented, D-shaped toroidal field (TF) coils. To keep the plasma stable, a helical total field is needed. It is obtained inductively, by driving a toroidal plasma current that creates a poloidal magnetic field component.

Tokamak plasmas are heated by self-heating provided by the fusion products such as alpha particles from the DT reaction, by Ohmic heating [33], by neutral beam injection (NBI) heating [34], and with radio frequency (RF) heating [35]. The Ohmic heating is present intrinsically, while NBI and RF heating power and deposition profiles can be controlled, with technological boundary conditions related to, e.g., available power.

The Ohmic heating becomes less efficient when the temperature rises, so these external heating mechanisms are needed to reach the fusion relevant temperatures.

To obtain fusion-relevant plasma discharges, a plasma with low density of the impurity particles are needed. Hence, the tokamak plasmas are operated in high vacuum conditions [36]. Gas puffing, pellet injection and pumping are main tools to fuel the plasma [37, 38] and to control the plasma density. Besides the TF coils, several other coils, both with poloidal and toroidal orientation, are used to control the plasma shape and stability.

The geometrical shape of the tokamak provides a symmetry along the toroidal or axial direction. Furthermore, the magnetic field forms concentric flux surfaces. From the first principles of plasma physics, it is known that many quantities such as the density, temperature and the pressure of the plasma are constant along these flux surfaces enabling, thereby, yet another symmetry. This reduces dimensions to only one, i.e. the flux surface.

In many cases, this 1D approximation is insufficient. For example, ITER has only 16 toroidal field coils. This breaks the toroidal symmetry and makes the magnetic field and the plasma genuine 3D objects. This is enhanced when the perturbations due to test blanket modules (TBMs) [39], neutral beam ports [40], ferritic inserts (FIs) [21], and ELM coils [41] are taken into account. Therefore, numerical models needed for realistically simulate fast ions in ITER require a full 3D description of the magnetic field.

2.1.2 Coordinate systems for a tokamak

Quantities, such as fast ion density or fast ion driven current density, are often given in the poloidal plane, illustrated in figure 2.1. In this figure, the plasma flux surfaces and the first wall of the ITER tokamak are shown as a function of the most important geometrical quantities, i.e. the major radius R and the vertical coordinate z. The flux surface coordinate for the 1D model is defined as the label for each surface with constant poloidal (toroidal) flux ψ_p (ψ_t), given by

$$\psi_t = \int \boldsymbol{B} \cdot \mathrm{d}\boldsymbol{a}_\phi \tag{2.1}$$

$$\psi_p = \int \boldsymbol{B} \cdot \mathrm{d}\boldsymbol{a}_\theta, \tag{2.2}$$

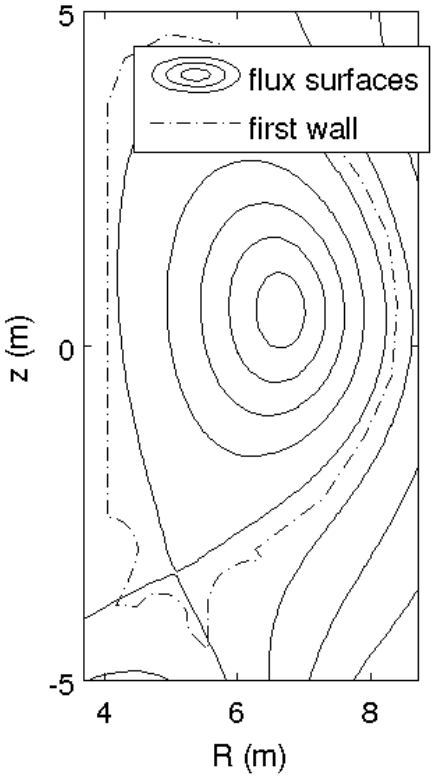

Figure 2.1. Plasma poloidal plane showing the flux surfaces and first wall of ITER tokamak.

where $\mathrm{d}\boldsymbol{a}_\theta$ and $\mathrm{d}\boldsymbol{a}_\phi$ are the differential area vectors with normals in the poloidal and toroidal directions, respectively. A Cartesian system of (x, y, z) can be used, while cylindrical coordinate system (R, ϕ, z) is more often utilized, here ϕ being the toroidal angle. The positive direction of the ϕ coordinate in this thesis is defined counter-clockwise when viewed from the top.

For theoretical considerations, and sometimes also for simulations, other coordinate systems are utilized. One of the examples is the so-called Boozer coordinate system [42], in which one of the coordinates is the poloidal flux and the two other coordinates are angular coordinates, i.e. (ψ, θ_B, ξ_B). With these field-aligned coordinates the field line becomes straight in the (θ_B,ξ_B)-plane. Moreover, the particle motion is very slow in the ψ_p direction compared to direction parallel to the magnetic field. Thus, particle orbits are generally faster to integrate using this coordinate system than with the Cartesian or cylindrical coordinate systems.

The drawback of this coordinate system is a divergence at the plasma separatrix, i.e. at the last closed flux surface the coordinate system is ill-defined. Therefore, this coordinate system cannot be used, e.g., to trace the particles crossing the separatrix or moving in the scrape-off layer.

2.2 Simulation model of the ASCOT code

Modern plasma physics is closely related to the computational physics. For example, to solve the Fokker-Planck equation [43] in a realistic 3D geometry, a numerical Monte Carlo scheme has to be utilized. The code used in this thesis, ASCOT [24], solves exactly this problem. It has been developed since 1990s within the research group at Helsinki University of Technology, nowadays Aalto University, and in VTT technological Research Center Finland. The code has been used earlier on for both fast ion related studies, e.g. [44–51], and, more recently, for impurity studies as well [52, 53].

ASCOT is a kinetic orbit-following guiding center code based on Monte Carlo method. Starting from the kinetic, the kinetic Fokker-Planck equation is solved, i.e.

$$\frac{\partial f_s}{\partial t} + \boldsymbol{v} \cdot \nabla f_s + \boldsymbol{a}_s \cdot \nabla_v f_s = C_s\left(f\right), \tag{2.3}$$

where $f_s = f_s\left(\mathbf{r}, \mathbf{v}, t\right)$ is the distribution function in the particle phase-space for species s, $\boldsymbol{a}_s = \frac{q_s}{m_s}\left(\boldsymbol{E} + \boldsymbol{v} \times \boldsymbol{B}\right)$ is the acceleration, and C_s is the collision operator in the particle phase-space.

A Monte Carlo method is applied because of the geometry of the system is complicated enough to motivate solving the equation by the test particle method and the fact that the collision operator is written in a Monte Carlo form. Each test particle trajectory is governed by the equations of motion, i.e. the orbits of the test particles are followed as discussed in [54].

Finally, the full Fokker-Planck equation, i.e. with the collision operator, is transformed from the particle phase-space to the guiding center phase-space, $(\boldsymbol{r}, \boldsymbol{v}) \Rightarrow \left(\boldsymbol{R}, v_{\parallel}, \mu, \chi\right)$. Hence, reduced guiding center kinetic equation is obtained

$$\frac{\partial F}{\partial t} + \dot{\boldsymbol{R}} \cdot \frac{\partial F}{\partial \boldsymbol{R}} + \dot{v}_{\parallel} \frac{\partial F}{\partial v_{\parallel}} = C_{GC}\left(F\right). \tag{2.4}$$

Here, instead of the particle distribution function f, we have introduced the reduced guiding center distribution function F. The collision operator

is transformed to the reduced guiding center phase-space and properly averaged over the gyro angle [54]. 'Reduced' here means that the guiding center transformed kinetic equation is further simplified by removing the fast gyro angle, χ, dependency from the equation. The resulting reduced guiding center phase-space is $(\boldsymbol{R}, v_\parallel, \mu)$, where $\boldsymbol{R}$ is the guiding center position, μ the magnetic moment and $v_\parallel$ the guiding center velocity parallel to the magnetic field.

The code is solving the kinetic equation rather than single particle trajectories. This is motivated by the connection of the kinetic equation with the stochastic differential equation [55]. These describe both the Hamiltonian motion and the drag/diffusion by the collisions with the background plasma for each phase-space coordinate. The kinetic equation is then solved by following the test particles according to stochastic differential equations, and constructing the distribution function from the test particle orbits. This procedure produces the solution to the kinetic equation (2.4). Distributions obtained this way are essentially velocity integrals of the reduced guiding center distribution function. More details can be found in the references [24, 54, 56].

2.2.1 Equations of motion

At the heart of any particle tracing code are the equations of motion describing the temporal evolution of the phase-space of the particle. To obtain statistically relevant results, large number of particles, up to several millions, has to be traced. Moreover, these high-energy particles are often followed until they are slowed down by the collisions with the background plasma. Hence, a guiding centre approximation is often applied to ease computational resources needed for the study.

The current ASCOT implementation is based on noncanonical Hamiltonian formulation derived from the Lie-transformed Lagrangian [15]

$$L = (q\mathbf{A} + m\mathrm{v}_\parallel \mathbf{b}) \cdot \dot{\mathbf{R}} + \frac{m\mu}{q}\dot{\chi} - H, \tag{2.5}$$

where $\mathrm{b} = \frac{\mathrm{B}}{B}$ is the magnetic field unit vector, χ is the gyro angle, and the Hamiltonian, H, is given by

$$H = \frac{1}{2} m \mathrm{v}_\parallel^2 + \mu B + q\Phi. \tag{2.6}$$

The guiding centre equations of motion are obtained by applying the Euler-Lagrange equation to the Lagrangian (2.5). This procedure yields the fol-

lowing set of equations [15]

$$\dot{\chi} = \frac{qB}{m}, \tag{2.7}$$

$$\dot{\mu} = 0, \tag{2.8}$$

$$\dot{\mathrm{v}}_{\parallel} = \frac{q}{m}\frac{\mathbf{B}^{\star}}{B^{\star}_{\parallel}} \cdot \mathbf{E}^{\star}, \tag{2.9}$$

$$\dot{\mathbf{R}} = \mathrm{v}_{\parallel}\frac{\mathbf{B}^{\star}}{B^{\star}_{\parallel}} + \mathbf{E}^{\star} \times \frac{\mathbf{b}}{B^{\star}_{\parallel}}, \tag{2.10}$$

where $B^{\star}_{\parallel} = \mathbf{B}^{\star} \cdot \mathrm{b}$, and the effective fields ($\mathbf{E}^{\star} = -\partial\mathbf{A}^{\star}/\partial t - \nabla\Phi^{\star}$, $\mathbf{B}^{\star} = \nabla \times \mathbf{A}^{\star}$) in Eqs. (2.9) and (2.10) are defined by the effective potentials

$$\Phi^{\star}(\mathbf{R}, \mu, t) = \Phi + \frac{\mu B}{q}, \tag{2.11}$$

$$\mathbf{A}^{\star}(\mathbf{R}, \mathrm{v}_{\parallel}, t) = \mathbf{A} + \frac{m\mathrm{v}_{\parallel}\mathbf{b}}{q}. \tag{2.12}$$

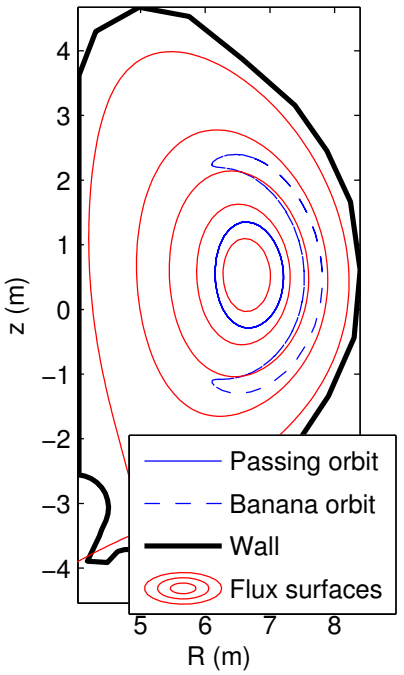

Figure 2.2. Examples of passing and trapped alpha particle orbits in the ITER geometry. The orbits are solved by the Runge-Kutta integration method.

To ensure solutions of high numerical accuracy, the integration scheme used to solve the equations of motion in ASCOT is the fourth order Runge-Kutta with a fifth order error prediction. The accuracy to which order the equations are solved is given as an input, and the implementation

takes care of adapting the time step to fulfill that accuracy. The guiding center motion is mathematically not a very stiff problem and it is solved by standard integrators with a high accuracy. In figure 2.2, a passing orbit and a trapped one are shown in ITER magnetic geometry.

The equations of motion are written in vector form and, hence, they are valid for all electromagnetic fields and integrable using any coordinate system. The crucial feature of ASCOT is the capability to use fully 3D magnetic field for particle tracing. As large data tables are needed for the magnetic data, the interpolation of this data becomes important. Firstly, the interpolation routine uses most of the CPU time and, therefore, an optimization of this part of the code is a very effective way to optimize the entire code. Secondly, any error in the magnetic field interpolation causes an error in the fast ion orbit tracing. Therefore, the interpolation scheme has stringent requirements for both speed and accuracy. In ASCOT, the field is interpolated using a free spline package PSPLINES [57].

2.2.2 Coulomb interactions and wall collision model

The Hamiltonian motion presented in the previous section does not describe the collisions between the traced guiding centers and other plasma particles. This effect is very important to take into account when studying phenomena with long temporal scales, e.g. in the simulations of wall power loads due to fast ions, or when the collisionality of fast ions is high.

In ASCOT, the collision operator is implemented in a Monte Carlo form and this operator acts on the guiding center phase-space coordinates. It is actually well-known that not only the velocity of the guiding center but also the position is changed in the collisions. The collisions are evaluated between the time steps and the guiding center phase-space is changed according to equations (32-33) and (42) shown in reference [24]. After each collision evaluation, a check is made to ensure that the collisions do not change the particle properties more than the user have defined in the input file. In case too large change is observed, the current time step is canceled and the next iteration is tried with halved time step.

To evaluate collisions, plasma kinetic profiles are needed. The standard set consists of temperature and density profiles, as shown in figures 2.3 and 2.4 for the 9 MA ITER scenario. The profiles are as a function of ρ_p, the normalized poloidal flux given by $\rho_p = \sqrt{(\psi - \psi_a) / (\psi_s - \psi_a)}$, where ψ_a/ψ_s are poloidal flux values at the magnetic axis/separatrix, respectively. In more advanced cases, 2D (R, z) profiles for the temperature and

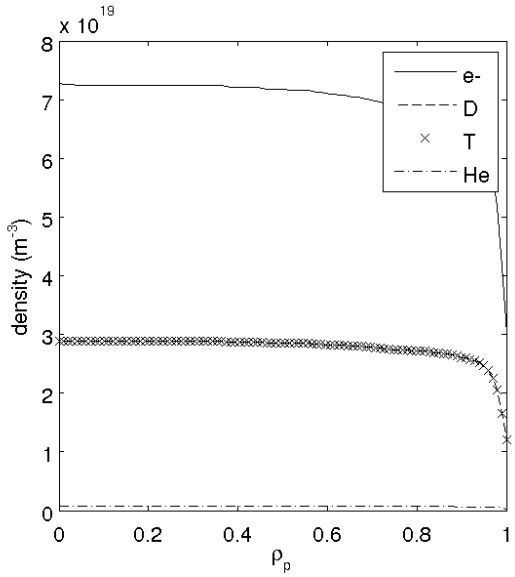

Figure 2.3. Plasma densities as a function of ρ_p for the 9 MA ITER scenario. Deuterium and tritium density lie on top of each other.

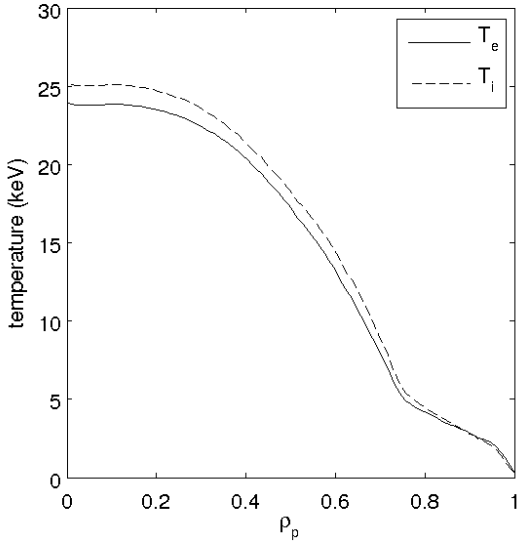

Figure 2.4. Electron and ion temperature as a function of ρ_p for the 9 MA ITER scenario.

density can be used. Optionally, the plasma rotation can be taken into account in the evaluation of the collisions. This is essential for the impurity studies, but not that important for the fast particles. The plasma rotation profile is, thus, an optional input for the code.

One of the crucial features of the ASCOT code is the fully 3D wall de-

sign allowing to study the wall loading in a realistic geometry with ports and protruding elements in the first wall. ASCOT uses a modified computer graphics implementation [58] to find an intersection of a line and a planar element, i.e. the particle orbit and the first wall. The accurate location together with the index of the wall tile in which the collision took place, is saved and stored for later use. The implementation has been found extremely reliable making sure that no particles are leaking from the region where the magnetic data is provided.

2.2.3 Running ASCOT on a (super)computer

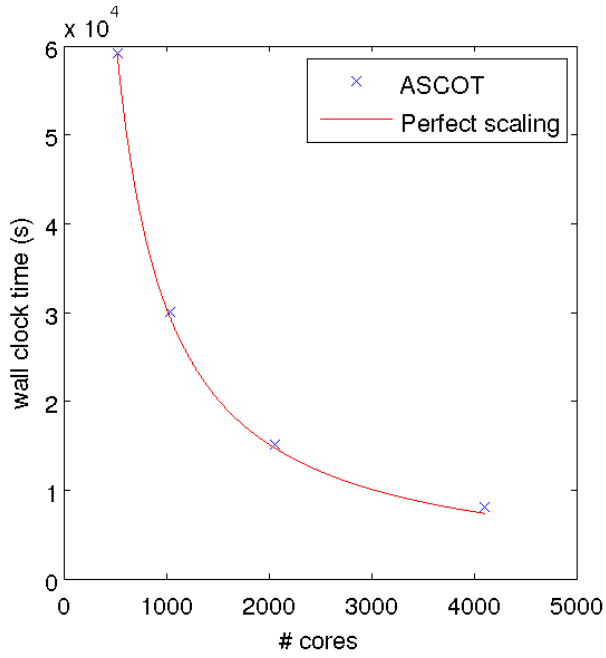

Figure 2.5. The scaling test of ASCOT in HELIOS supercomputer. As is shown, ASCOT scales nearly ideally as the test particles can be simulated independent of each other.

ASCOT source code is written in FORTRAN90 and can be compiled either on standard desktop machine or in supercomputer clusters, such as HELIOS [59] and CSC [60]. The only library needed for the compilation, besides the commonly available libraries for MPI routines, is HDF5 [61] and it is routinely available on major supercomputers. In case ASCOT is operated in the supercomputer environment, batch scripts are available to define the job configuration to be sent to the batch queue and later on to the computing cores.

As each test particle in an ASCOT simulation is independent from the other test particles, the code scales nearly perfectly with the number of cores as shown in figure 2.5. In a typical run of 300 000 alpha particles traced for roughly a second in ITER lasts up to 20 hours on the HELIOS supercomputer using up to 4096 processes, or 256 cores.

The generation of ASCOT input data is usually done using a set of MATLAB routines that construct separate ASCII-files for the magnetic field, the kinetic plasma profiles and the first wall. The ASCOT toolbox contains a separate program to evaluate and produce a file for the initial locations of the test particles, whether guiding centers or full orbit particles. The program includes a neutral beam particle model [62] for various tokamaks, fusion product model for the most common fusion reactions, and a simplified model for ICRH particles (see reference [24]). The ASCOT run is controlled by an input file defining the simulation parameters, e.g., the end criteria and the output that is produced during the run.

3. Development of numerical models

This chapter presents the development of numerical models. First, an alternative particle tracing method, dubbed full orbit tracing, to the guiding center following was introduced. This new method can be used to both ensure that the guiding center approximation is valid and to substitute the guiding center formalism in situations where it cannot be applied.

The second half of the development provided ASCOT with a model for the interaction of fast particles with MHD instabilities like NTMs and TAEs. In this chapter, the most important numerical development is summarized. Some additional tests, not included in the related publications, are presented here for the first time.

3.1 Full orbit particle tracing

As derived in section 2.2.1, the guiding center transformation is often used to ease the computational effort. It is, however, applicable only when the following criteria are met

$$\rho_L \frac{\nabla B}{B} \ll 1 \tag{3.1}$$

$$\frac{\Omega}{B}\frac{\partial B}{\partial t} \ll 1, \tag{3.2}$$

where $\Omega = qB/m$ and ρ_L are the characteristic temporal and spatial scales, respectively, of the charged particle gyration around the magnetic field line. Hence, the criteria reads that the magnetic field cannot change too much within a Larmor radius ρ_L or within the time it takes for a particle to complete a single Larmor gyration. The same applies to all the other fields needed for particle tracing, e.g. the electric field or kinetic profiles needed for the evaluation of the collisions with the background plasma.

If the criteria are not met, the gyro motion of the particle must be resolved in order to get reliable results. A good example of this is the fusion

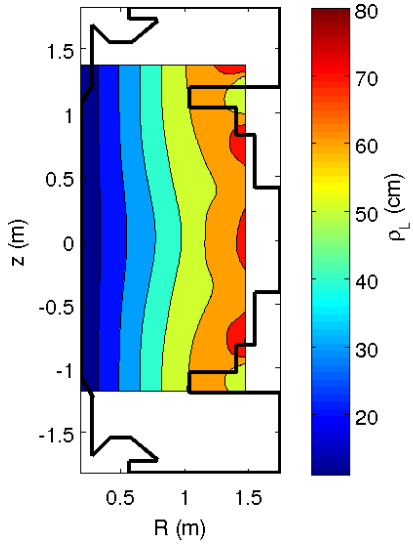

Figure 3.1. The Larmor radius of 3 MeV fusion protons in the magnetic field of the MAST tokamak. The usage of the guiding center approximation is very ambiguous for this plasma.

products in Mega Ampere Spherical Tokamak (MAST) for which the Larmor radius in the poloidal plane is shown in figure 3.1. It is concluded that the guiding center approximation can not be very accurate in this case as the Larmor radius can be close to a half of the minor radius. To address such plasmas and to assess how large of an error is done using the guiding center approximation, an option to trace the full particle orbits was introduced to ASCOT code as described in Publication I. Moreover, periodic TF ripple perturbations may cause additional transport only seen in the full particle orbits as explained in [63].

It was noticed that, for time scales relevant for the energetic particle in ITER, following the full particle motion is a significant computational task for two reasons. Firstly, the problem is mathematically stiff and, therefore, special attention must be paid in the way the equations of motions are solved. Secondly, even with valid numerical implementation the computational task can be 50-100 times more demanding than with the guiding center approximation, as was explained in Publication II. Despite the computational costs, the model presented in Publication I has already been used in many studies [48–51, 64].

The motion of a charged particle in a general electromagnetic field is

described by the equations of motion

$$\dot{\mathbf{v}} = \frac{q}{m}\left(\mathbf{E} + \mathbf{v} \times \mathbf{B}\right), \tag{3.3}$$

$$\dot{\mathbf{r}} = \mathbf{v}. \tag{3.4}$$

To solve these equations for non-trivial electromagnetic fields, a numerical integration algorithm must be introduced. The standard integration method to solve differential equations is Runge-Kutta. Routinely, the fourth order Cash-Karp Runge-Kutta with fifth order error monitoring is used for particle tracing applications. The well-known disadvantage of using Runge-Kutta for this problem is the energy conservation, i.e., the integration method does not conserve the test particle energy. The error is proportional to the length of the integration time step. Hence, the user is forced to limit either the length of the time steps or the simulation time.

However, using a modified one step Leap Frog scheme instead of higher order Runge-Kutta methods, and given by

$$\mathbf{v}_{i+1} = \mathbf{v}_i + \Delta t \frac{q}{m}\left(\mathbf{E}_i + \frac{\mathbf{v}_{i+1} + \mathbf{v}_i}{2} \times \mathbf{B}_i\right) \tag{3.5}$$

$$\mathbf{r}_{i+1} = \mathbf{r}_i + \Delta t \mathbf{v}_i \tag{3.6}$$

as suggested in Publication I and [65], ensures the conservation of the total energy in the absence of electric field. This can be shown by a direct calculation: first, the equation (3.5) is solved for $\mathbf{v}_{i+1}$ by taking a cross product with $\mathbf{B}$ and rearranging the terms to arrive with an expression

$$\mathbf{v}_{i+1} = -\mathbf{v}_i + 2\frac{\mathbf{v}_i + \mathbf{v}_i \times \tilde{\mathbf{B}} + \frac{(\mathbf{v}_i \cdot \tilde{\mathbf{B}})\tilde{\mathbf{B}}}{4}}{1 + \frac{\tilde{B}^2}{4}}, \tag{3.7}$$

where $\tilde{\mathbf{B}} = \frac{\Delta t q \mathbf{B}}{m}$. This equation is dotted with itself giving

$$v_{i+1}^2 = \mathbf{v}_{i+1} \cdot \mathbf{v}_{i+1} \tag{3.8}$$

$$= v_i^2 - 4\frac{\mathbf{v}_i \cdot \mathbf{v}_i + \frac{\left(\mathbf{v}_i \cdot \tilde{\mathbf{B}}\right)^2}{4}}{1 + \frac{\tilde{B}^2}{4}} \tag{3.9}$$

$$+ 4\frac{\mathbf{v}_i \cdot \mathbf{v}_i + 2\frac{\left(\mathbf{v}_i \cdot \tilde{\mathbf{B}}\right)^2}{4} + \frac{\left(\mathbf{v}_i \times \tilde{\mathbf{B}}\right) \cdot \left(\mathbf{v}_i \times \tilde{\mathbf{B}}\right)}{4} + \frac{\left(\mathbf{v}_i \cdot \tilde{\mathbf{B}}\right)\tilde{B}^2}{16}}{\left(1 + \frac{\tilde{B}^2}{4}\right)^2}, \tag{3.10}$$

where the term (3.10) can be decomposed according to $(\mathbf{a} \times \mathbf{b}) \cdot (\mathbf{a} \times \mathbf{b}) = a^2 b^2 - (\mathbf{a} \cdot \mathbf{b})^2$.

Hence, (3.10) reads as

$$4\frac{\mathbf{v}_i\cdot\mathbf{v}_i+2\frac{\left(\mathbf{v}_i\cdot\tilde{\mathbf{B}}\right)^2}{4}+\frac{\mathbf{v}_i\cdot\mathbf{v}_i\tilde{B}^2-\left(\mathbf{v}_i\cdot\tilde{\mathbf{B}}\right)^2}{4}+\frac{\left(\mathbf{v}_i\cdot\tilde{\mathbf{B}}\right)\tilde{B}^2}{16}}{\left(1+\frac{\tilde{B}^2}{4}\right)^2} \tag{3.11}$$

$$=4\frac{\mathbf{v}_i\cdot\mathbf{v}_i\left(1+\frac{\tilde{B}^2}{4}\right)+\frac{\left(\mathbf{v}_i\cdot\tilde{\mathbf{B}}\right)\tilde{B}^2}{4}\left(1+\frac{\tilde{B}^2}{4}\right)}{\left(1+\frac{\tilde{B}^2}{4}\right)^2} \tag{3.12}$$

$$=4\frac{\mathbf{v}_i\cdot\mathbf{v}_i+\frac{\left(\mathbf{v}_i\cdot\tilde{\mathbf{B}}\right)^2}{4}}{1+\frac{\tilde{B}^2}{4}}. \tag{3.13}$$

Using this result, expression (3.8) can be simplified to $v_{i+1}^2 = v_i^2$, i.e. the energy of the particle is explicitly conserved using this scheme. This enables longer time steps and longer simulation times.

Another major advantage of the Leap Frog method comes from the faster evaluation of the equations of motion. Using, e.g., fifth order Runge-Kutta method as is used in ASCOT, the electromagnetic fields need to be interpolated five times more often than in the Leap Frog implementation. Hence, the calculation becomes rapidly much more CPU time consuming.

To demonstrate this, ASCOT was used to calculate the full orbit motion of a 3.5 MeV alpha particle in an axisymmetric magnetic field of ITER using both Leap Frog and Kash-Karp Runge-Kutta methods. The particle was followed in both cases for 10 ms and the time step was selected to be on the average 0.5 μs. Using a standard desktop computer, the evaluation took roughly 22 minutes and 36 seconds with Leap Frog method, while the computing time was 36 minutes and 39 second when Runge-Kutta was used, i.e. the computation time increased by 62 %. Changing to a 3D magnetic field, where the interpolation becomes heavier, the computing times were 27 minutes, 19 seconds for Leap Frog and 52 minutes, 52 seconds for Runge-Kutta. Thus Runge-Kutta took almost twice the CPU time required by Leap Frog.

The energy is conserved within 1 % when the test particle was traced by Runge-Kutta integration for 10 ms. Increasing the time step leads to a situation where the test particle energy starts to rapidly drift, eventually leading to also a spatial drift and lost orbit. Hence, the time step used for Runge-Kutta solution was close to the maximum value that can be used for an acceptable solution. For Leap-Frog method, the time step can be safely increased to 5 μs with the orbit unchanged within the numerical accuracy, giving even more edge for the Leap Frog method over the Runge-Kutta. The kinetic energy conservation using different methods and different time steps is demonstrated in Figure 3.2.

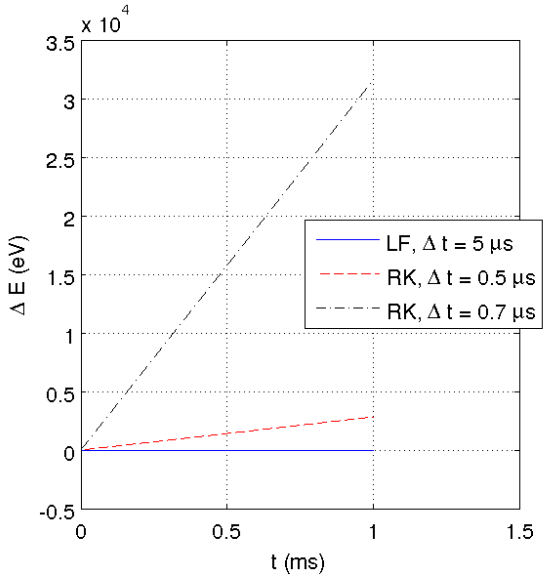

Figure 3.2. The change of the kinetic energy of the alpha particle, from the initial 3.5 MeV, using different full orbit methods and time steps. With Leap Frog (LF), the energy is explicitly conserved but with Runge-Kutta (RK) the energy starts to drift in case a too large time step is used. Therefore, the time stepping for Runge-Kutta has to be small enough to conserve the energy of the particle for the needed simulation time.

3.2 Magnetohydrodynamical instabilities

In the presence of MHD activities, the traditional guiding center simulations can not explain the observed losses of fast ions nor the confined fast ion density in the plasma. Moreover, in many experiments [66–71], a large number of different MHD instabilities have been observed and they are expected to be present in the future burning plasmas as well. Hence, running fast ion simulations to model these cases, the effect of MHD instabilities have to be taken into account. Therefore, several fast ion codes, e.g. SPIRAL [25] and HAGIS [30], have been developed to include the effects of MHD modes on fast ions.

MHD modes generate a perturbation to the electromagnetic fields that affect the particle motion. The particle motion itself can be a substantial driver for the modes and, hence, particles act back to the modes resulting in a complex nonlinear wave-particle interaction. Taking into account the full interaction is not possible without either using approximations or coupling many simulation tools together. An example of the former is HAGIS code that takes into account the interaction of the particles and

waves with the approximation that the wave mode structure is fixed, i.e. the fast ion drive alters only the amplitude of the prescribed eigenstructure of the waves. This eigenstructure is usually calculated by a separate code. A more consistent approach includes coupling of the eigenstructure solver to the kinetic solver enabling to solve the non-linear saturation of both the amplitude and the structure of the waves.

In ASCOT, the wave-particle interaction is modeled by the electromagnetic perturbations affecting the particle motion and neglecting the effect of the fast particles to the waves. This means that the non-linear mode evolution is not calculated and essentially only a single time slice with predetermined mode structure is simulated. However, the ASCOT model provides inclusion of the modes together with an arbitrary 3D magnetic field, the realistic vacuum region and a fully 3D wall design. These are often neglected in more self-consistent approaches. With these approximations, ASCOT provides a tool to estimate the fast ion response to prescribed MHD perturbation in a realistic magnetic configuration.

The model for the MHD modes is based on adding the perturbation to the magnetic and electric potentials. The structure of the modes is helical in field-aligned coordinates (θ_B, ξ_B), i.e.

$$\alpha = \sum_{nm} \alpha_{nm}(\psi_p) \sin\left(n\xi_B - m\theta_B - \omega_{nm}t\right), \tag{3.14}$$

$$\tilde{\Phi} = \sum_{nm} \tilde{\Phi}_{nm}(\psi_p) \sin\left(n\xi_B - m\theta_B - \omega_{nm}t\right), \tag{3.15}$$

where the magnetic part of the perturbation is $\tilde{\boldsymbol{B}} = \alpha \boldsymbol{B}$ and the electric part is given by $\tilde{\Phi}$.

The novel part of the model is that one can use any coordinate system for the particle tracing and evaluate the perturbations using coordinate transformations from these coordinates to the field-aligned ones. Hence, there is actually no restriction on the coordinate system for the particle following as long as coordinate transformations are available. Moreover, the particle crossing the separatrix can be simulated using this approach. The equations of motion (2.7-2.10) remain the same but the effective potentials are slightly modified by the perturbations

$$\Phi^{\star\star}(\mathbf{R}, \mu, t) = \Phi^{\star} + \tilde{\Phi}, \tag{3.16}$$

$$\mathbf{A}^{\star\star}(\mathbf{R}, \mathrm{v}_{\parallel}, t) = \mathbf{A}^{\star} + \alpha \mathbf{B}. \tag{3.17}$$

Thus in the numerical implementation, evaluation of α, $\nabla\alpha$, $\tilde{\Phi}$ and $\nabla\tilde{\Phi}$ are needed in the coordinate system the particle orbits are solved in. In AS-

COT, the coordinate transformations from cylindrical/toroidal coordinates to field-aligned coordinates and back are used.

This model is valid as long as the symmetry is helical and the approximation for the parallel magnetic vector potential can be used. This is generally true for all low-β MHD modes such as toroidal Alfvén eigenmodes (TAEs) and neoclassical tearing modes (NTMs). For NTMs, the α_{nm} parameter can be given by theory-motivated parametrization(s) [72, 73] or by external MHD calculations. For the Alfvénic modes, either α_{nm} or $\tilde{\Phi}_{nm}$ can be given and the other is calculated from the condition of vanishing parallel electric field as electrons rapidly smooth out any potential gradients along the magnetic field. Vanishing $E_\parallel$ yields the connection between α and $\tilde{\Phi}$

$$E_\parallel = \omega B \alpha_{nm} \cos\left(n\xi_B - m\theta_B - \omega t\right) - \frac{\mathbf{B}\cdot\nabla\tilde{\Phi}}{B} = 0 \tag{3.18}$$

$$\Rightarrow \alpha_{nm} = \frac{(nq-m)}{\omega\left(gq-I\right)}\Phi_{nm}, \tag{3.19}$$

where the functions g and I are known coefficients of the covariant representation of $\mathbf{B}$, i.e.

$$\mathbf{B} = g\left(\psi_p\right)\nabla\xi_B + I\left(\psi_p\right)\nabla\theta_B + \delta\nabla\psi_p \tag{3.20}$$

and q is the safety factor. The parallel electric field vanishes due to rapid mobility of the electrons along the field line. In case this assumption is not valid due to, e.g., very intense local heating, both α_{nm} and $\tilde{\phi}_{nm}$ must be given as input.

In the ASCOT implementation, the MHD modes are included as follows. The axisymmetric part of the magnetic field is used to generate the coordinate transformation from field-aligned coordinates to cylindrical coordinates and back. In the same process the functions g, q and I are tabulated and converted to spline objects. Thereafter, the particles are followed and during every time step, α, $\nabla\alpha$, $\tilde{\Phi}$ and $\nabla\tilde{\Phi}$ are evaluated using the splines. The guiding center equations of motion are solved in the presence of the fully 3D magnetic field. The implementation is discussed in more detail in Publication IV.

4. Results of numerical simulations

This chapter discusses the results of numerical simulations carried out using the new numerical models introduced to ASCOT. In section 4.1, the ITER wall power loads, calculated with full orbit following, are presented, while section 4.2 reports on the current and torque driven by fusion alphas in ITER. Section 4.3 presents detailed benchmarking, verification and validation studies that have not been reported earlier. In section 4.4, the effect of MHD modes on fast ions is addressed.

4.1 ITER wall power loads with full orbit tracing

In ITER, the approximation of axisymmetry for the magnetic field is broken at several levels. The 18 toroidal field coils break the axisymmetry while retaining 18-fold symmetry. This periodic perturbation is referred to as TF ripple. The remaining pieces of symmetry are broken by the perturbations caused by the ferritic materials, such as neutral beam ports and TBMs. Due to these asymmetries in the magnetic field, the guiding center theory is only an approximation. Figure 4.1 represents the Larmor radius for 3.5 MeV alpha particles in the realistic magnetic field of ITER. The Larmor radii are evaluated at the toroidal location $\phi = 0$ assuming the velocity is purely perpendicular to the magnetic field. From this figure, it is not obvious whether there is any difference to use full orbit following instead of guiding center following. Therefore, numerical simulations investigating this issue are needed.

This was done for the case where ITER wall power load by alphas was simulated using both full orbit and guiding center integration methods. A set of simulations was carried out for the 9 MA advanced scenario with central reversed shear using different models for particle tracing. Not only pure guiding center (pure GC) and pure full orbit tracing (pure FO)

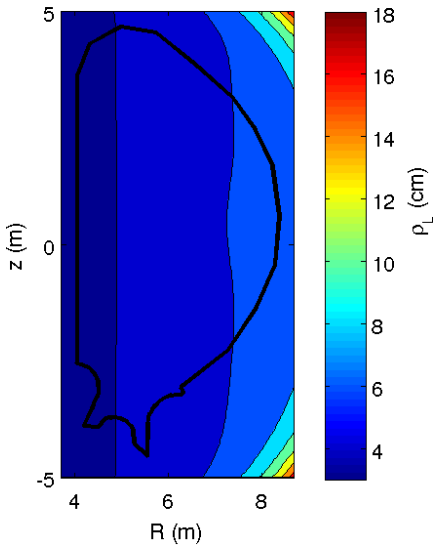

Figure 4.1. The Larmor radius of 3.5 MeV alpha particles in the 3D magnetic field of ITER containing TF ripple and perturbations due to TBMs, neutral beam ports and ELM coils. The validity of the guiding center theory needs to be checked with numerical simulations.

were used, but also a hybrid model (GC+FO) was considered. In this model the guiding centers are simulated away from the walls and full orbit solution is used only in the vicinity of the walls. In the simulations, 110 000 test alpha particles with an energy of 3.5 MeV were followed until they hit a wall element or slow down to 100 keV. The magnetic data together with the corresponding kinetic plasma profiles were imported from the ITER database (IDM reference number 27JSKQ).

The simulated wall power loads as a function of the toroidal angle are shown in figure 4.2. Pure FO results in a higher wall load compared to guiding center based methods. The GC+FO method estimates the wall loads much more accurately, statistically, than pure GC method while keeping the computational costs very limited compared to those of pure FO.

For guiding center methods, the error bars for the wall loads are shown. The errors are estimated from statistically independent samples, in this case six different ensembles of 110 000 alphas were used, and calculating the variance of the sample mean. Hence, an estimate for the Monte Carlo errors made in the simulations with 68 % confidence level are obtained. The uncertainty for the pure GC case at the peak heat power load location around the outer midplane (poloidal angle of 0 °) is below 5 %. The total

Quantity	Pure GC	GC + FO	Pure FO
Total power (kW)	8.51	18.20	20.00
Peak power (kW/m^2)	2.54	5.17	12.55
Loss fraction (%)	0.033	0.056	0.064

Table 4.1. The total power to the wall, the peak power load and the alpha loss fraction for ITER scenario 4 from three different orbit-following methods.

power to the wall, the peak power and the loss power fraction for the three different orbit-following options are given in table 4.1. It is observed that pure GC produce lower total power load while the two other methods are very close to each other. The main reason why pure GC differs so drastically from the other two is the fact that the GC center path is a distance of Larmor radius further away from the wall. The difference between the GC+FO and pure FO methods is explained by the additional transport induced by the FO following, e.g. the enhanced TF ripple diffusion [63].

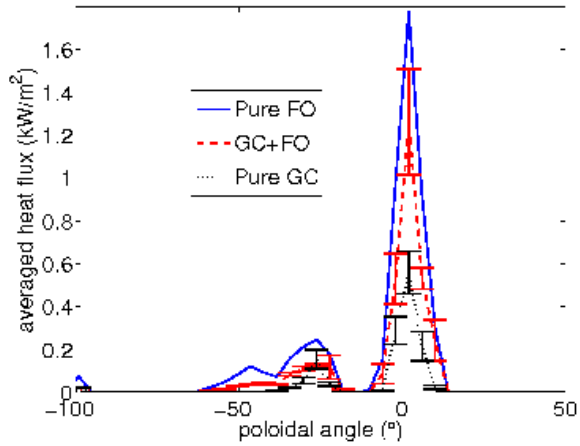

Figure 4.2. Toroidally averaged wall power loads for ITER scenario 4 alpha particles. The heat loads are obtained for pure GC simulation (black dotted line), hybrid simulation (red dashed line) and pure FO simulation (blue solid line).

In Publication II, it was also concluded that, in the case studied, the full orbit following is on the average 70-100 times more CPU intensive than the ordinary guiding center following. Moreover, the hybrid method was found to produce very similar results as the guiding center following while retaining the computation time effectively at the guiding center level. Even in the case when pure FO method was used, the wall loads stayed well within the design limits of ITER.

4.2 Alpha particle current and torque drive in ITER

The tokamak principle is based on the inductively driven plasma current to obtain the poloidal component of the helical magnetic field. For a fusion power plant, the pulsed operation is not feasible to maintain a high duty cycle and, hence, several non-inductive methods to drive the plasma current have been proposed.

The friction between passing particles and precessing trapped particles leads to a toroidal net current, called the bootstrap current [74–78]. Depending on the equilibrium and the kinetic plasma profiles, the bootstrap current can add up to 70 % [79] of the total plasma current needed for steady-state operation. It is important to note the intrinsic nature of this process.

The fusion-born alpha particles can also generate bootstrap current via this mechanism. The energy (and, thus, the speed) of alphas is roughly 350 times higher than for the thermal particles, but their density is lower. As with the fuel ions, the alpha particle bootstrap current depends very strongly on the equilibrium conditions. In the presence of a so-called current hole, the alpha particle current can be up to 20 % of the total plasma current [80].

In addition to non-inductively driven current, plasma rotation is considered very important as it has several beneficial effects on tokamak plasmas, for example sheared flows has been observed to suppress the turbulence and plasma rotation is observed to stabilize external MHD modes [81–84]. Rotation can be driven by inducing a torque to the plasma. Conventionally, this is accomplished by toroidally directed neutral particle injection.

The total torque is composed of two components. Collisions change the momentum of the particles and, therefore, contribute as a collisional component. Secondly, the fast ions are leaking from the plasma into the scrape-off layer, resulting in a radial current. The thermal plasma responds to this current with an inward return current to cancel the charge separations. As a result, there is a $j \times B$ -component for the total torque. Only the toroidal component of the torque vector is considered.

The alpha particle driven current and torque have previously been estimated by analytical calculations [85] and by numerical simulations [80, 86, 87] with consistent outcome: the alpha particle current will be small compared to the total plasma current, and the alpha-driven torque is ef-

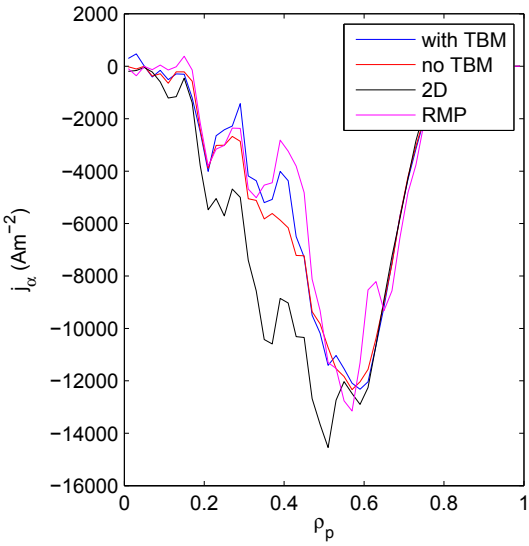

Figure 4.3. The alpha particle net toroidal current density in the 9 MA scenario. Four different magnetic configurations are considered. The current density is roughly independent of the magnetic configuration.

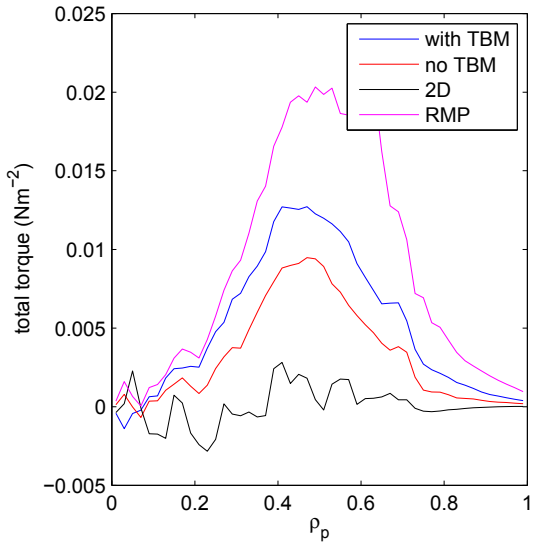

Figure 4.4. The alpha particle total torque density in the 9 MA scenario. Four different magnetic configurations are considered. The torque is nonzero only for 3D magnetic configurations.

fectively zero as the collisional and $j \times B$ components cancel. However, all these studies have assumed axisymmetric magnetic field which is not the case for ITER with the ripple magnitude of 0.5-2%, depending on the

magnetic configuration.

To assess the impact of non-axisymmetry on additional fast ion transport, ASCOT simulations were carried out for four different magnetic configurations and two of the ITER baseline scenarios. The magnetic field configurations include axisymmetric case (2D) for comparison and benchmarking with the earlier work, 3D versions including the TF ripple and ferritic inserts both with (TBM) and without (no TBM) a perturbation due to test blanket modules. Finally, the TBM configuration was further modified by the resonant magnetic perturbation due to ELM coils (RMP).

The RMP case was calculated using the vacuum approximation. In this magnetic field even the thermal plasma is not confined [51]. The idea to introduce this partially unphysical magnetic field configuration was to study the effect of significant alpha particle losses on the current and torque densities. These four configurations were considered for both the 9 MA advanced reversed shear and the 15 MA standard Q=10 H-mode ITER scenario.

In the simulations, 300 000 alphas were followed until their energy slowed down to local thermal temperature, they hit a wall element or slowed down below 1 keV. Essential part of the work was the update of the electron shielding model that is described in Publication V. This enabled to evaluate the net current density from the gathered fast ion current density.

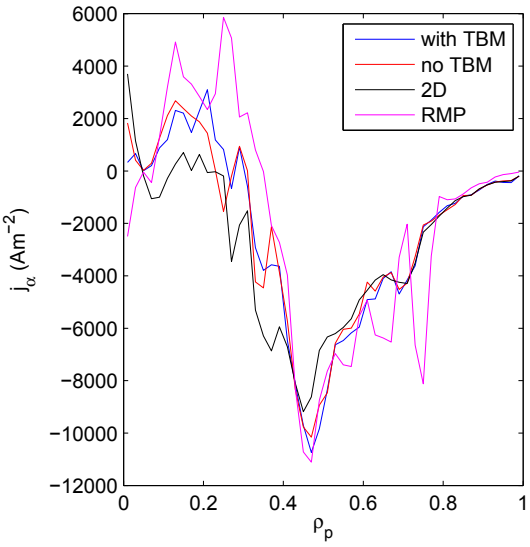

Figure 4.5. The alpha particle net toroidal current density in the 15 MA scenario.

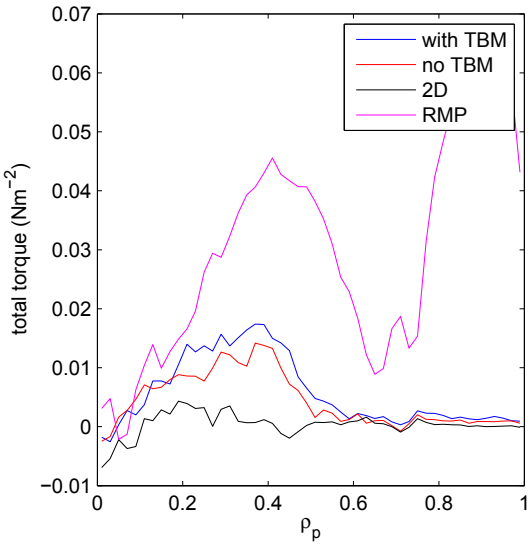

Figure 4.6. The alpha particle total torque density in the 15 MA scenario.

The net alpha particle current for both scenarios is by most parts independent on the 3D nature of the magnetic configuration, while for the total torque density the non-axisymmetry plays a significant role. This is illustrated in figures 4.3 and 4.4 for the 9 MA scenario and in figures 4.5 and 4.6 for the 15 MA scenario. For the axisymmetric cases, the torque components are found to cancel each other, as suggested by the earlier works. For the non-axisymmetric cases, the increased fast ion transport leads to a non-zero torque density. The alpha particle torques peak radially inward compared to peaks of the 3D perturbations. The reason for this is, that there are only limited amount of alpha particles at the plasma edge, where the perturbations peak. However, there are much more particles in the core region and the lower perturbation amplitude still results in larger transport and, thus, torque in the core region.

According to tables 4.3 and 4.3, all integrated alpha particle currents are below one percent of the total plasma current. As for the case of the induced torques, the numbers for alpha particles are opposite in sign compared to the NBI particles, and order of magnitude smaller. As majority of the beam ions has the same initial direction, the guiding centers of the beam ions are all located inwards from the initial particle positions. This contribution, negative in sign, has a major effect on the NBI torque, while for alphas the guiding centers are both inward and outward from the initial particle positions and the net effect averages to zero.

Configuration	Net fast-ion current (kA)	Total fast ion torque (Nm)
alpha TBM	-61	3.2
alpha no TBM	-62	2.0
alpha 2D	-74	0.11
alpha RMP	-59	6.0
on-axis NBI TBM	-520	-6.5
off-axis NBI TBM	-470	-4.3
on-axis NBI no TBM	-520	-6.1
off-axis NBI no TBM	-470	-3.9
on-axis NBI 2D	-520	-6.1
off-axis NBI 2D	-470	-3.7
on-axis NBI RMP	-520	-8.7
off-axis NBI RMP	-470	-6.5

Table 4.2. Integrated fast ion torques and currents using different magnetic configurations for alpha particles and NBI particles in the 9 MA ITER scenario. Negative sign implies co-current direction.

Configuration	Net fast-ion current (kA)	Total fast ion torque (Nm)
alpha TBM	-48	2.9
alpha no TBM	-47	2.0
alpha 2d	-50	0.31
alpha RMP	-47	33
on-axis NBI TBM	-570	-16
off-axis NBI TBM	-470	-15
on-axis NBI no TBM	-570	-16
off-axis NBI no TBM	-470	-15
on-axis NBI 2D	-560	-17
off-axis NBI 2D	-460	-16
on-axis NBI RMP	-540	6.6
off-axis NBI RMP	-460	6.5

Table 4.3. Integrated fast ion torques and currents using different magnetic configurations for alpha particles and NBI particles in the 15 MA ITER scenario. Negative sign implies co-current direction.

4.3 Benchmarking, verification and validation of the MHD model in ASCOT

The effect of the MHD instabilities on the fast particles is important because of these modes may induce additional fast ion losses to the walls. Moreover, possible redistribution of fast particles inside the plasma due to MHD modes may cause unwanted behaviour in the main plasma, e.g. the current drive and energy deposition profiles might be redistributed which then leads to a change in the plasma heating.

The fast particles act as a driver for certain MHD instabilities, such as TAEs, and the interplay between the modes and the particles must be understood to control the burning plasmas. ITER will be the first tokamak in which the burning plasma conditions are achieved and, therefore, these issues will be experimentally faced for the first time. Self-consistent alpha particle physics is not studied in this thesis. However, the effect of MHD perturbations on the fast ion distribution function and the fast ion induced wall power loads in the presence of a realistic 3D magnetic field have been investigated.

In this section, the usage of the MHD model in ASCOT for the predictive simulations in ITER is motivated by testing the model. For the most parts, this material have not been published in a peer-reviewed paper.

The MHD model in the ASCOT code was benchmarked against the HAGIS code, that is mature enough to be considered as a reference, [30] for the transport of the fast particles in the presence of MHD modes, in this case a neoclassical tearing mode. The HAGIS code has been used in this kind of studies earlier on. To be able to benchmark single particle trajectories with high accuracy, attention must be paid to ensure that both of the codes are using the very same magnetic field for the particle tracing.

In this case, both codes were able to read in same file format, so using the same file was possible. The data is, however, processed inside HAGIS before it is used for the particle tracing. To make sure that the data for particle tracing is the same for both codes, the poloidal flux difference between the two codes was evaluated and is shown in figure 4.7. As seen, the poloidal flux is found to be identical to fractions of promille in the plasma region, which guarantees that the poloidal magnetic field is the same. The toroidal component was checked separately using the flux-function $F = RB_\phi$.

As a first step, the particle orbits were compared in MHD-quiescent

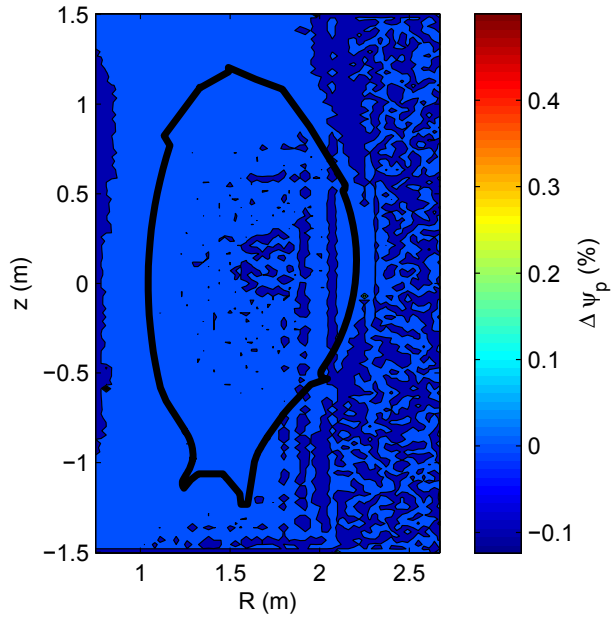

Figure 4.7. The difference in the poloidal magnetic flux seen by the ASCOT and HAGIS codes. As a conclusion, the codes are using the same magnetic field.

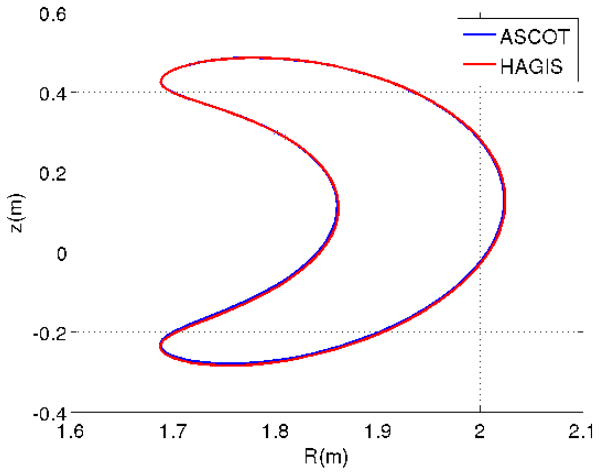

Figure 4.8. Comparison of a particle orbit calculated by the ASCOT and HAGIS codes. There is no essential difference between the two.

plasma, as shown in figure 4.8. The orbits are not identical but within less than a millimeter from each other. The small discrepancy comes from the fact that the two codes solve the noncanonical Hamiltonian equations of motion in different coordinate systems. In ASCOT, the cylindrical co-

ordinates are used, whereas HAGIS uses the field-aligned coordinates. Moreover, the interpolation of the magnetic data is handled differently. Both orbits seems to be stable, which should be the case in a 2D magnetic field.

A (3,2) NTM perturbation was applied in both of the codes and the trace of the test particle in poloidal cross-section was compared. As shown in figure 4.9, under the influence of a NTM perturbation the orbits start to differ more than in axisymmetric case, but still less than a centimeter. As even a small discrepancy between the orbits leads to a different perturbations at the particle positions, these small discrepancies tend to grow. This explains why the perturbed orbits are not matching as good as the unperturbed ones.

Also definition of the mode differs between the codes: ASCOT uses $\alpha_{nm}(\psi_p)$ as an input and HAGIS $\phi_{nm}(\psi_p)$. Even though effort was put to make sure the perturbations seen by the two codes were the same, some small discrepancies rising from, e.g., the interpolation schemes were not possible to resolve.

A similar procedure was done also for TAEs, as presented in Publication IV. There not only the single particle orbits, but also the kinetic energy was compared as the electric field perturbation changes the test particle kinetic energy. Correspondence within less than a percent was obtained between the two codes. As a conclusion, the MHD model in ASCOT has a correct form for the perturbation fields and the code produce very similar orbits as HAGIS code does.

In order to validate the codes, both codes were used to simulate real experimental results from AUG tokamak. In the shot # 20853, ECE measurements with modulated beam power suggested a depletion of up to 60 % of the beam ion density at the resonance surface of a (3,2) NTM mode. This conclusion was reached by assuming that the beam particles transfer their energy via collisions to electrons and thus the modulation in the beam power is reflected to the electron temperature. ASCOT and HAGIS codes were then used to analyze the case.

As HAGIS does not have Coulomb collisions, 200 000 collisionless deuterium beam particles were used by both codes to gather the radial density profile with and without the effect of the (3,2) NTM perturbation. In figure 4.10, the relative change of the beam density is compared. Both codes produce similar density depletion but much smaller than expected from the measurements, i.e. of the order of 5 % rather than 60 %. However,

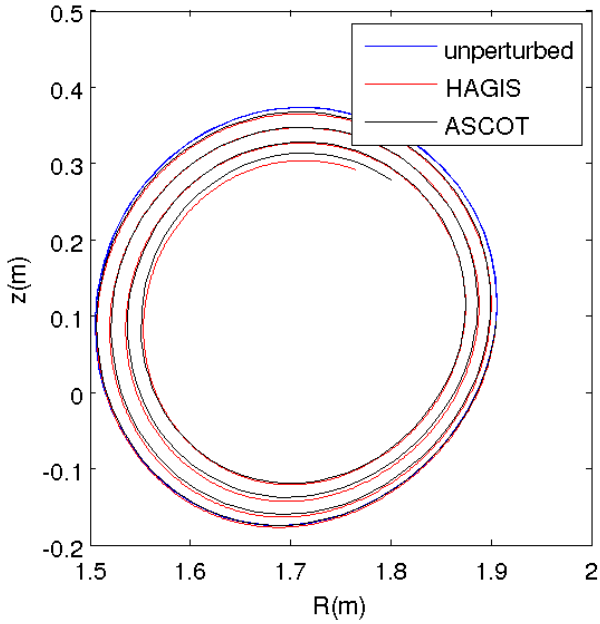

Figure 4.9. Comparison of particle orbits with (3,2) NTM perturbation calculated using ASCOT and HAGIS codes, and MHD queiescent particle orbit calculated by ASCOT.

the profile of the relative density difference has a dip at the location of the resonance surface around $\rho_p = 0.4$, as was also indicated by the measurements and the shape of the density profiles are very similar for both codes.

Regarding all the differences between the two codes, the correspondence found here was agreed to be sufficient for benchmarking. From the validation point of view, it was agreed with the experimental team that the interpretation of the experimental measurements is wrong, i.e. simulations carried out here do not support the massive beam density depletion. It was left for future work to study whether, e.g., the heat transport in the presence of the NTM could explain the missing piece from the puzzle. As a result, it was concluded that the validation of the codes needs to be carried out using different experimental set-up, and it was left as a future work. Knowing that HAGIS has been used successfully to model the effect of MHD modes on fast particles, this analysis was considered sufficient to carry on with the predictive NTM simulations for ITER using the NTM model in ASCOT.

Further verification studies were done for the TAE wave-particle reso-

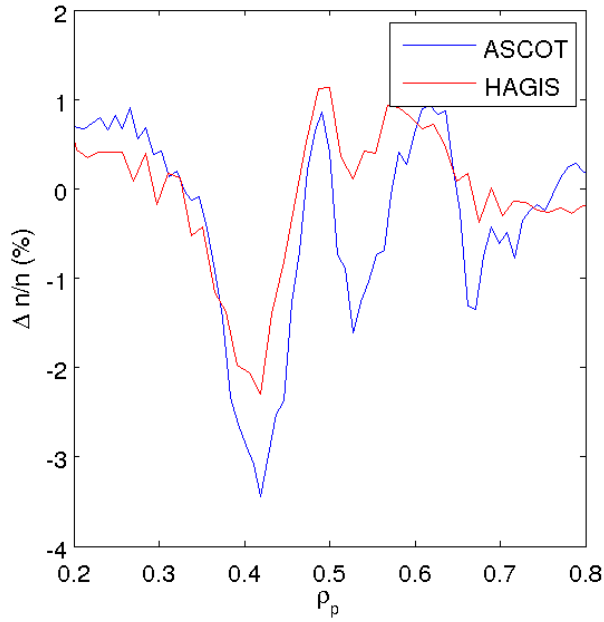

Figure 4.10. Comparison of relative change in beam ion density with and without the (3,2) NTM perturbation. The simulations by ASCOT and HAGIS agree well qualitatively, and decently quantitatively.

nances. The AUG shot #25491 at $t = 0.78$ s was selected as an equilibrium. At this time slice, a $f = 140$ kHz TAE mode with $n = 6$ was observed by the magnetics, and associated losses of beam ions were measured by the fast ion loss detector (FILD) [88], see figure 13 in [89].

To locate the wave-particle resonances, ASCOT simulations were carried out. In the simulations, 1 000 000 test particles from NBI source #8 were followed for 1 ms and collisions were turned off. The resulting velocity-space of the guiding center particles was compared with and without TAE perturbations in figure 4.11. This figure is from spatial location ($R = 1.69$ m, $z = -0.23$ m). A wave-particle resonance is observed just below $E = 93$ keV and around $\xi = 0$. The wave-particle resonance is associated with a change in the test particles energy.

A condition for the wave-particle resonances can be written as

$$\Omega_{np} = \omega - n\omega_t - p\omega_p \approx 0, \tag{4.1}$$

here Ω_{nm} is the resonance width, ω is the frequency of the mode ($\omega = 2 * \pi * f$), ω_t is the toroidal frequency of the particle, and ω_p is the poloidal orbit frequency. To find possible resonances from the given equilibrium, a suitable ensemble of particles can be launched and the toroidal and

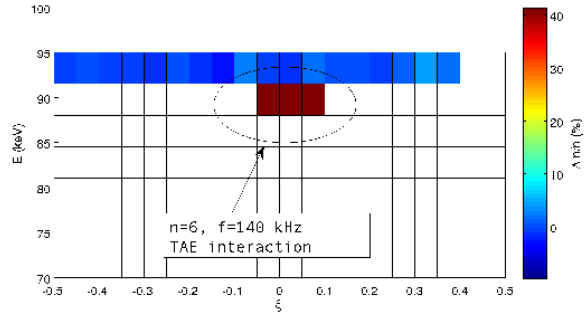

Figure 4.11. Relative difference of the beam ion density with and without n=6 TAE as a function of energy and pitch angle. The figure is zoomed to the full energy of the beams and region of wave-particle interaction is highlighted.

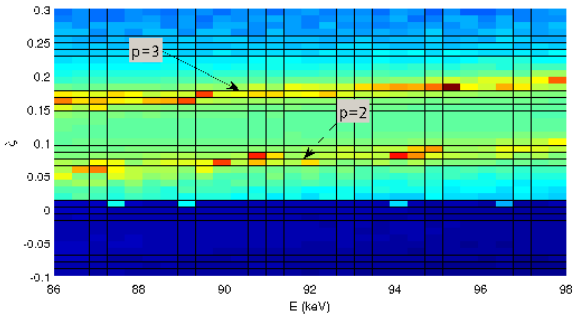

Figure 4.12. Logarithm of the inverse wave-particle resonance width, i.e. $\log\left(|1/\Omega_{np}|\right)$, identifies resonances from the shown velocity space and associates them with the wave-particle interaction seen in the ASCOT simulations.

poloidal frequencies can be calculated from the particle orbits. The resonances are determined by plotting $\log\left(|1/\Omega_{np}|\right)$ as a function of the selected phase-space.

For the above mentioned case, the frequency calculation was done at the same spatial location, changing the energy and pitch of the particle around the observed resonance. The result is shown in figure 4.12, where two possible resonances are identified with poloidal mode numbers $p = 2, 3$. Both of these may cause the energy exchange seen in figure 4.11. This verifies that the resonance found from the analytical expression for the resonance condition can be found from the full ASCOT simulation with the interaction of particles with the TAE waves.

The wave-particle interaction can be associated with a spatial redistribution of the particles. This spatial redistribution can be connected with

a change in the particles energy [90] as

$$\frac{d\psi_p}{dt} = -\frac{mg - nI}{\omega D}\frac{dE}{dt}, \tag{4.2}$$

where $D = gq + I + \rho_{\parallel}(gI' - Ig')$, g and I are flux functions calculated from the magnetic field, and primes indicate differentiation with respect to ψ_p. The spatial redistribution corresponding to figure 4.11 is shown in figure 4.13. Measuring this redistribution experimentally is challenging as usually the mode perturbation amplitudes are small and the level of redistribution is below 10 %, which typically is a limit for measuring confined fast ions by, e.g. fast-ion D-alpha (FIDA) [91] or collective Thompson scattering (CTS) measurements [92]. However, were the redistribution to happen close to the plasma edge, it would be associated with the fast ion losses and measurable by the FILD detector.

For this particular case, the losses were measured and the result is shown in figure 13 of reference [89]. Using ASCOT, a synthetic FILD diagnostic can be used. For this case, the particle number was rather limited and only a few particles hit the synthetic detector plate in its actual position. Hence, instead of selecting particles that hit the real FILD location, all lost particles were used to build the figure 4.14. The dominating spot in the FILD detector plate is seen also in the ASCOT simulations at around ($\rho_L = 3$ cm $, v_{\parallel}/v = 40^{\circ}$). More detailed analysis, with the collisions turned on, will be carried out in the future for a shot with better diagnostic coverage enabling possible even to measure the confined fast ions by means of tomography [93, 94].

4.4 The effect of NTMs and TAEs on fast ions in ITER

The effect of several MHD instabilities, including NTMs and TAEs, on fast particles have been studied numerically in great detail in the recent years [66, 68, 73, 95, 96]. In all of these studies, the magnetic field is either assumed axisymmetric or an analytical approximation of the real 3D field has been used. However, more recently serious concerns regarding the effect of non-axisymmetric magnetic fields on fast particle transport [41, 47, 97, 98] have been expressed. Therefore, ASCOT simulations with both MHD instabilities and non-axisymmetric realistic 3D magnetic fields included in the simulations were carried out for ITER. The results of these simulations for alpha particles are reported in detail in Publication III, while the NBI particle simulations are published here for the first

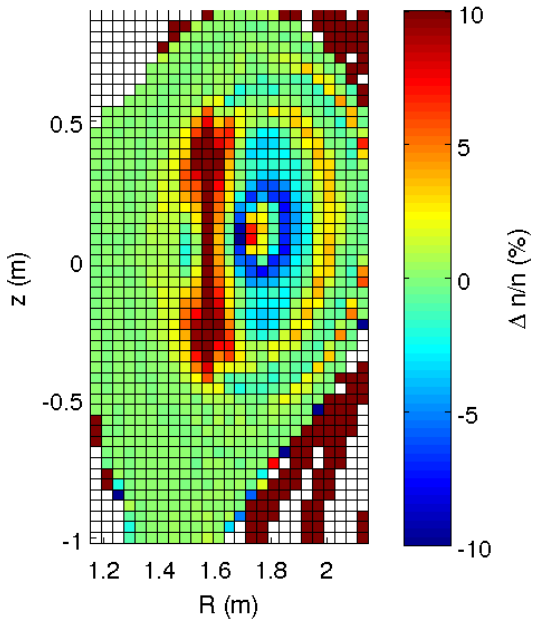

Figure 4.13. The spatial redistribution of the beam ions in the presence of $n = 6$ TAE mode in the ASDEX Upgrade tokamak.

time but they have been presented, e.g., in the ITPA meeting.

The simulations for NTMs were carried out for the 15 MA baseline ITER scenario using a realistic 3D magnetic field and kinetic plasma profiles from the ITER database (IDM reference number 27JSKQ). In the simulations, 100 000 alpha particles with initial energy of 3.5 MeV were followed until they were slowed down to the local temperature, hit a wall element or until their energy dropped below 1 keV. Both (2,1) and (3,2) NTMs were simulated and the radial profile used in the simulations is described in detail in Publication III. In the simulations, the NTMs were assumed static.

As the amplitude of the NTMs was increased, an increase in the wall power loads was observed, see figure 4.15. However, even using island widths exceeding the mitigation threshold of 10 cm and even above locked-mode threshold of 20 cm [99, 100], the wall power load stayed within the design limit of 0.5 MW/m^2 (for the main wall) [101]. Assuming that the NTMs will be mitigated to widths below 10 cm, the wall power loads are insignificant.

As for the neutral beam ions, the beam deposition in ITER is quite deep in the plasma, while for the 15 MA scenario the q-profile is such that the most important NTMs (2,1) and (3,2) are located further out in the

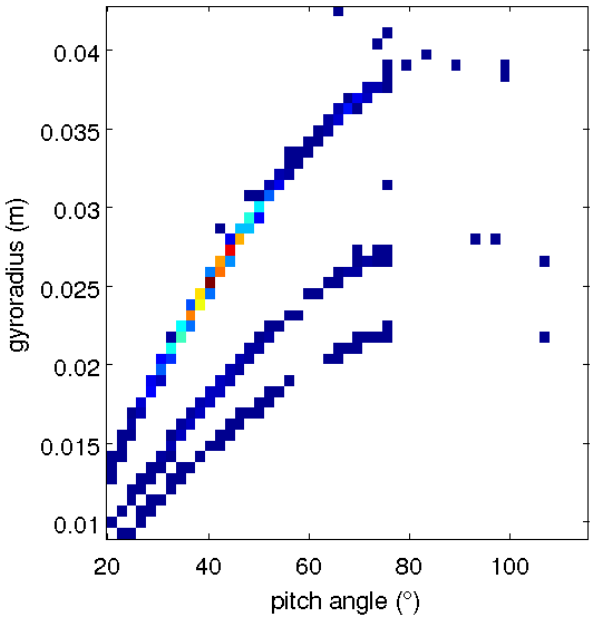

Figure 4.14. The velocity space distribution of lost particles calculated from the ASCOT simulation with $n = 6$ TAE mode. The gyroradius is a measure of the particle energy. The definition of the pitch angle ξ is modified to $180^\circ - \xi$ to ease the comparison with the experimental FILD measurements that use this definition.

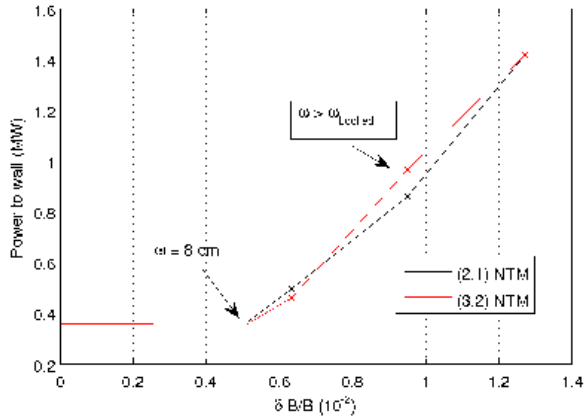

Figure 4.15. Total alpha particle power to the first wall as a function of the amplitude of (3,2) and (2,1) NTM perturbations. The perturbations related to the island width of locked modes and the threshold for NTM mitigation are indicated.

plasma. Hence, no drastic effect on wall power loads, energy deposition nor current drive was observed.

For TAEs, the advanced 9 MA reversed shear ITER scenario was stud-

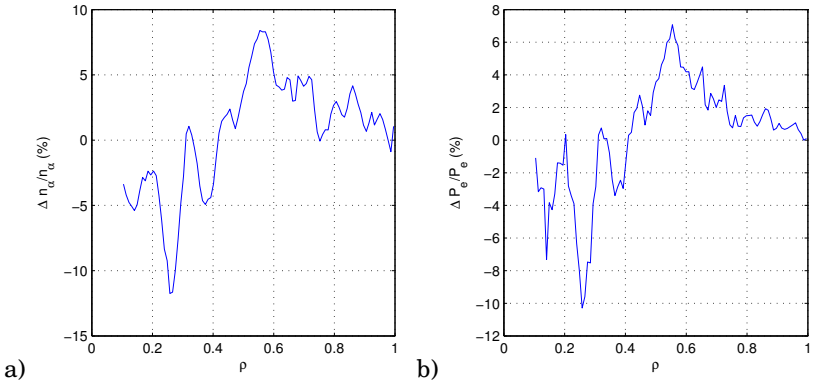

Figure 4.16. (a) The simulated relative change in the alpha density, brought about by the $n = 5$ TAE modes, as a function of ρ_p. (b) The simulated relative power deposition difference from alpha particles to electrons between the case with the TAE present and the case with no TAE.

ied, motivated by [96] were TAE activity was found more severe for this scenario compared to the 15 MA scenario. The eigenstructure of the modes was calculated by the LIGKA code [102] and the most unstable mode with $f = 51.5$ kHz and $n = 5$ was considered in the simulations. The eigenstructure is shown in figure 6 of Publication III. As these TAE modes are rotating, this need to be taken into account when initializing the particles. This is done in ASCOT by assigning a random phase for each test particle. To address this 200 000 test particles were followed with the same end conditions as was used for the NTM case.

For both alphas and NBI particles, no drastic effect on the wall power loads was found, while redistribution inside the plasma was observed. The redistribution for alphas was found to alter both the density and the heat deposition profiles by 10 % in figure 4.16. Moreover, changes in the fast ion velocity space were reported in Publication III. For NBI particles, the current drive profile was modified by the TAE mode and resulted in a drop in the current density around $\rho_p \approx 0.2 - 0.3$, see figure 4.17.

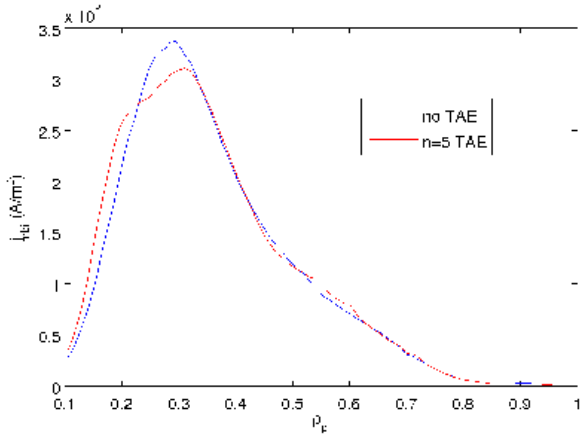

Figure 4.17. The current density from NBI ions as a function of ρ_p for the cases with and with out n=5 TAE. Current density redistribution is clearly seen.

5. Summary, discussion and outlook

5.1 Summary and discussion

The goal of this thesis work was to bring the orbit-following simulations of fast ions in tokamaks two steps closer to reality. The first half of the thesis dealt with the full orbit motion and the validity of the guiding center approximation. Publication I describes the upgrade of the ASCOT code with an option to follow full orbits. The latter part of the thesis is dedicated to the effect of MHD modes on fast particles. A numerical model to asses the effect of MHD modes on fast particles in a realistic 3D magnetic field was implemented in the ASCOT code in Publication IV.

Different orbit-following models were applied in standard ASCOT simulations calculating the alpha particle wall load in ITER. It was found that the guiding center approximation holds well enough and the full orbit effects can be introduced by a hybrid method following guiding centers in the core of the plasma and switching to full orbit following only in the vicinity of the walls. This hybrid method allows both statistically accurate and acceptable wall clock time for the simulation in the same package. Based on the work presented in Publication I and Publication II, this option has been used in the majority of ASCOT simulations.

The new model for MHD modes in ASCOT was carefully verified against theory and a benchmark was carried out against the HAGIS code as discussed in 4.3. The model was applied to study the effect of NTMs and TAEs on fast particles in ITER resulting in Publication III and Publication IV.

For NTMs with realistic amplitudes, the effect to fast ion spatial profile was found to be insignificant. Moreover, the fast ion wall loads remained within the design limits for the first wall even with unrealistically large

mode amplitudes. For TAEs, a 10% response was found for the fast ion spatial profile, leading to roughly 10 % changes in the alpha particle energy deposition profile, the alpha particle density profile and the neutral beam driven current density profile.

While for NTMs the results can be considered general, the case of TAEs is more complex. Even a slight change in the plasma equilibrium can change the eigenstructure, and thereby the induced transport. Therefore, further studies are presently carried out to fully understand how the TAEs affect the fast ion transport in the whole operational regime of ITER. The results obtained in this thesis for TAEs should, for the above mentioned reasons, be considered more an exploratory result than a general result.

Last but not least, in Publication V, the ASCOT simulation model was used to understand the alpha particle driven current and torque in ITER baseline scenarios with realistic 3D magnetic field. It was found that the alpha driven current will be below one percent of the total plasma current in all simulated cases, while the alpha particle driven torque was found to not to vanish in the presence of a 3D magnetic field. The alpha particle torque was found to be in opposite direction and an order of magnitude smaller than the torque induced by the neutral beam particles. Therefore, unfortunately, alpha particles are predicted not to drive significant amount of rotation.

5.2 Outlook

Even though many issues were studied in this thesis, further work focuses, for example, on the *validation* of the MHD model is yet to be carried out. An effort to that direction has already been initiated. ASCOT has recently been used to explain the expulsion of fast ions from the core of ASDEX Upgrade in the presence of a (1,1) kink mode. These experiments have been carried out in ASDEX Upgrade, and their results will be presented in future publications. FIDA-measurements clearly show that the fast ion density is depleted at the resonance surface of the kink mode. Guiding center simulations by TRANSP/NUBEAM [103, 104] and ASCOT simulations without the MHD modes can not explain this depletion. With the kink mode included in ASCOT simulations, however, a clear depletion of fast ions from the resonance surface is observed. Using the simulation results, a synthetic diagnostic signal using FIDASIM code [105] will be

obtained and compared to the actual FIDA signal.

When high-n or high-m number TAE modes are simulated, the validity of the guiding center approximation needs to be assessed. For these situations, an improved method for the particle tracing needs to be applied. The part of the Lagrangian that breaks down the guiding center approximation has to be separated and perturbation theory needs to be used. As a result, equations of motion will reflect the ones obtained by the gyro kinetic theory, i.e. the rapidly changing part of the Lagrangian has to be evaluated by taking averages along the gyro orbit. Models of gyro-averaged TAE modes will be implemented to ASCOT code, allowing simulations for high-n TAE modes which are expected to dominate in burning plasmas.

In the simulations described in this thesis, the vanishing parallel electric field approximation has been used for all Alfvénic simulations. A set of simulations investigating the validity of this approximation will be carried out in the future. In these simulations, the approximation is relaxed by taking both the electric and magnetic part of the perturbation as input, i.e. α_{nm} and $\tilde{\Phi}_{nm}$.

Moreover, the interplay between the fast ion transport due to Alfvénic modes and neoclassical transport will be investigated by carrying out simulations with and without Coulomb collisions. Previously the collisional transport has often been neglected from the MHD induced transport simulations, e.g. [89, 106]. The collisions is expected to feed particles to the wave-particle resonances, and thus increase the fast ion transport.

Finally, the rotation of NTMs and kink modes will be implemented in ASCOT as described in [107]. The effect of induced electric field on the fast ion transport will be studied using cases presented in this thesis, allowing existing data points for non-rotating NTMs to compare with the rotating ones.

Bibliography

[1] Catherine Wolfram, Orie Shelef, and Paul J. Gertler. How will energy demand develop in the developing world? Working Paper 17747, National Bureau of Economic Research, January 2012.

[2] ITER Physics Basis Editors, ITER Physics Expert Group Chairs, Co-Chairs, ITER Joint Central Team, and Physics Integration Unit. Chapter 1: Overview and summary. *Nuclear Fusion*, 39(12):2137–2174, 1999.

[3] R. Hiwatari, K. Okano, Y. Asaoka, K. Shinya, and Y. Ogawa. Demonstration tokamak fusion power plant for early realization of net electric power generation. *Nuclear Fusion*, 45(2):96, 2005.

[4] J D Lawson. Some criteria for a power producing thermonuclear reactor. *Proceedings of the Physical Society. Section B*, 70(1):6, 1957.

[5] J. D. Huba. NRL Plasma Formulary. Naval Research Laboratory, Washington, D.C., 2006.

[6] M.M. Basko, A.J. Kemp, and J. Meyer ter Vehn. Ignition conditions for magnetized target fusion in cylindrical geometry. *Nuclear Fusion*, 40(1):59, 2000.

[7] G. Y. Fu, R. Nazikian, R. Budny, and Z. Chang. Alpha particle-driven toroidal Alfvén eigenmodes in Tokamak Fusion Test Reactor deuterium-tritium plasmas: Theory and experiments. *Physics of Plasmas (1994-present)*, 5(12):4284–4291, 1998.

[8] Heating ITER Physics Expert Group on Energetic Particles, Current Drive, and ITER Physics Basis Editors. Chapter 5: Physics of energetic ions. *Nuclear Fusion*, 39(12):2471, 1999.

[9] A. Fasoli, C. Gormenzano, H.L. Berk, B. Breizman, S. Briguglio, D.S. Darrow, N. Gorelenkov, W.W. Heidbrink, A. Jaun, S.V. Konovalov, R. Nazikian, J.-M. Noterdaeme, S. Sharapov, K. Shinohara, D. Testa, K. Tobita, Y. Todo, G. Vlad, and F. Zonca. Chapter 5: Physics of energetic ions. *Nuclear Fusion*, 47(6):S264, 2007.

[10] H. Alfvén. On the motion of a charged particle in a magnetic field. *Arkiv Mat. Astr. Fysik*, 1940.

[11] Theodore G Northrop. *The adiabatic motion of charged particles*, volume 21. Interscience publishers New York, 1963.

[12] R.G. Littlejohn. A guiding center Hamiltonian: A new approach. *Journal of Mathematical Physics*, 20(12):2445–2458, 1979.

[13] R.G. Littlejohn. Hamiltonian perturbation theory in noncanonical coordinates. *Journal of Mathematical Physics*, 23(5):742–747, 1982.

[14] R.G. Littlejohn. Variational principles of guiding centre motion. *Journal of Plasma Physics*, 29:111–125, 2 1983.

[15] J.R. Cary and A.J. Brizard. Hamiltonian theory of guiding-center motion. *Rev. Mod. Phys.*, 81:693–738, May 2009.

[16] F. L. Hinton and R. D. Hazeltine. Theory of plasma transport in toroidal confinement systems. *Rev. Mod. Phys.*, 48(2):239–308, Apr 1976.

[17] R. B. White and M. S. Chance. Hamiltonian guiding center drift orbit calculation for plasmas of arbitrary cross section. *Physics of Fluids (1958-1988)*, 27(10):2455–2467, 1984.

[18] S. Günter, G. Conway, S. daGraça, H.-U. Fahrbach, C. Forest, M. Garcia Muñoz, T. Hauff, J. Hobirk, V. Igochine, F. Jenko, K. Lackner, P. Lauber, P. McCarthy, M. Maraschek, P. Martin, E. Poli, K. Sassenberg, E. Strumberger, G. Tardini, E. Wolfrum, H. Zohm, and ASDEX Upgrade Team. Interaction of energetic particles with large and small scale instabilities. *Nuclear Fusion*, 47(8):920, 2007.

[19] M.H. Redi, M.C. Zarnstorff, R.B. White, R.V. Budny, A.C. Janos, D.K. Owens, J.F. Schivell, S.D. Scott, and S.J. Zweben. Collisional stochastic ripple diffusion of alpha particles and beam ions on TFTR. *Nuclear Fusion*, 35(10):1191, 1995.

[20] R.V. Budny. A standard DT supershot simulation. *Nuclear Fusion*, 34(9):1247, 1994.

[21] K. Shinohara, S. Sakurai, M. Ishikawa, K. Tsuzuki, Y. Suzuki, K. Masaki, O. Naito, K. Kurihara, T. Suzuki, Y. Koide, T. Fujita, Y. Miura, and the JT-60 Team. Ferritic insertion for reduction of toroidal magnetic field ripple on JT-60U. *Nuclear Fusion*, 47(8):997, 2007.

[22] K. G. McClements. Full orbit computations of ripple-induced fusion alpha-particle losses from burning tokamak plasmas. *Physics of Plasmas*, 12(7):072510, 2005.

[23] V. A. Yavorskij, Zh. N. Andrushchenko, J. W. Edenstrasser, and V. Ya Goloborod'ko. Three-dimensional Fokker–Planck equation for trapped fast ions in a Tokamak with weak toroidal field ripples. *Physics of Plasmas*, 6(10):3853–3867, 1999.

[24] E. Hirvijoki, O. Asunta, T. Koskela, T. Kurki-Suonio, J. Miettunen, S. Sipilä, A. Snicker, and S. Äkäslompolo. ASCOT: Solving the kinetic equation of minority particle species in tokamak plasmas. *Computer Physics Communications*, 185(4):1310 – 1321, 2014.

[25] G J Kramer, R V Budny, A Bortolon, E D Fredrickson, G Y Fu, W W Heidbrink, R Nazikian, E Valeo, and M A Van Zeeland. A description of the full-particle-orbit-following spiral code for simulating fast-ion experiments in tokamaks. *Plasma Physics and Controlled Fusion*, 55(2):025013, 2013.

[26] R.J. Akers, E. Verwichte, T.J. Martin, S.D. Pinches, and R. Lake. GPGPU Monte Carlo Calculation of Gyro-Phase Resolved Fast Ion and n-State Resolved Neutral Deuterium Distributions. In *Proc. 39th EPS Conference on Plasma Physics*, Europhysics Conference Abstracts, page P5.088, Stockholm, Sweden, 2012.

[27] R.J. Akers, L.C. Appel, P.G. Carolan, N.J. Conway, G.F. Counsell, M. Cox, S.J. Gee, M.P. Gryaznevich, R. Martin, A.W. Morris, M.P.S. Nightingale, A. Sykes, M. Mironov, and M.J. Walsh. Neutral beam heating in the START spherical tokamak. *Nuclear Fusion*, 42(2):122, 2002.

[28] A. Fasoli, D. Borba, B. Breizman, C. Gormezano, R. F. Heeter, A. Juan, M. Mantsinen, S. Sharapov, and D. Testa. Fast particles-wave interaction in the Alfvén frequency range on the Joint European Torus tokamak. *Physics of Plasmas (1994-present)*, 7(5):1816–1824, 2000.

[29] M. García-Muñoz, H.-U. Fahrbach, S. Günter, V. Igochine, M. J. Mantsinen, M. Maraschek, P. Martin, P. Piovesan, K. Sassenberg, and H. Zohm. Fast-Ion Losses due to High-Frequency MHD Perturbations in the ASDEX Upgrade Tokamak. *Phys. Rev. Lett.*, 100:055005, Feb 2008.

[30] S.D. Pinches, L.C. Appel, J. Candy, S.E. Sharapov, H.L. Berk, D. Borba, B.N. Breizman, T.C. Hender, K.I. Hopcraft, G.T.A. Huysmans, and W. Kerner. The HAGIS self-consistent nonlinear wave-particle interaction model. *Computer Physics Communications*, 111(1-3):133 – 149, 1998.

[31] H.-S. Bosch, R.C. Wolf, T. Andreeva, J. Baldzuhn, D. Birus, T. Bluhm, T. Bräuer, H. Braune, V. Bykov, A. Cardella, F. Durodié, M. Endler, V. Erckmann, G. Gantenbein, D. Hartmann, D. Hathiramani, P. Heimann, B. Heinemann, C. Hennig, M. Hirsch, D. Holtum, J. Jagielski, J. Jelonnek, W. Kasparek, T. Klinger, R. König, P. Kornejew, H. Kroiss, J.G. Krom, G. Kühner, H. Laqua, H.P. Laqua, C. Lechte, M. Lewerentz, J. Maier, P. McNeely, A. Messiaen, G. Michel, J. Ongena, A. Peacock, T.S. Pedersen, R. Riedl, H. Riemann, P. Rong, N. Rust, J. Schacht, F. Schauer, R. Schroeder, B. Schweer, A. Spring, A. Stäbler, M. Thumm, Y. Turkin, L. Wegener, A. Werner, D. Zhang, M. Zilker, T. Akijama, R. Alzbutas, E. Ascasibar, M. Balden, M. Banduch, Ch. Baylard, W. Behr, C. Beidler, A. Benndorf, T. Bergmann, C. Biedermann, B. Bieg, W. Biel, M. Borchardt, G. Borowitz, V. Borsuk, S. Bozhenkov, R. Brakel, H. Brand, T. Brown, B. Brucker, R. Burhenn, K.-P. Buscher, C. Caldwell-Nichols, A. Cappa, A. Cardella, A. Carls, P. Carvalho, Ł. Ciupiński, M. Cole, J. Collienne, A. Czarnecka, G. Czymek, G. Dammertz, C.P. Dhard, V.I. Davydenko, A. Dinklage, M. Drevlak, S. Drotziger, A. Dudek, P. Dumortier, G. Dundulis, P.v. Eeten, K. Egorov, T. Estrada, H. Faugel, J. Fellinger, Y. Feng, H. Fernandes, W.H. Fietz, W. Figacz, F. Fischer, J. Fontdecaba, A. Freund, T. Funaba, H. Fünfgelder, A. Galkowski, D. Gates, L. Giannone, J.M. García Regaña, J. Geiger, S. Geißler, H. Greuner, M. Grahl, S. Groß, A. Grosman, H. Grote, O. Grulke, M. Haas, L. Haiduk, H.-J. Hartfuß, J.H. Harris, D. Haus, B. Hein, P. Heitzenroeder, P. Helander, R. Heller, C. Hidalgo, D. Hildebrandt, H. Höhnle, A. Holtz, E. Holzhauer, R. Holzthüm, A. Huber, H. Hunger, F. Hurd, M. Ihrke, S. Illy, A. Ivanov, S. Jablonski, N. Jaksic, M. Jakubowski, R. Jaspers, H. Jensen, H. Jenzsch, J. Kacmarczyk, T. Kaliatk, J. Kallmeyer, U. Kamionka, R. Karaleviciu, S. Kern, M. Keunecke, R. Kleiber, J. Knauer, R. Koch, G. Kocsis, A. Könies,

M. Köppen, R. Koslowski, J. Koshurinov, A. Krämer-Flecken, R. Krampitz, Y. Kravtsov, M. Krychowiak, G. Krzesinski, I. Ksiazek, M. Kubkowska, A. Kus, S. Langish, R. Laube, M. Laux, S. Lazerson, M. Lennartz, C. Li, R. Lietzow, A. Lohs, A. Lorenz, F. Louche, L. Lubyako, A. Lumsdaine, A. Lyssoivan, H. Maaßberg, P. Marek, C. Martens, N. Marushchenko, M. Mayer, B. Mendelevitch, Ph. Mertens, D. Mikkelsen, A. Mishchenko, B. Missal, T. Mizuuchi, H. Modrow, T. Mönnich, T. Morizaki, S. Murakami, F. Musielok, M. Nagel, D. Naujoks, H. Neilson, O. Neubauer, U. Neuner, R. Nocentini, J.-M. Noterdaeme, C. Nührenberg, S. Obermayer, G. Offermanns, H. Oosterbeek, M. Otte, A. Panin, M. Pap, S. Paquay, E. Pasch, X. Peng, S. Petrov, D. Pilopp, H. Pirsch, B. Plaum, F. Pompon, M. Povilaitis, J. Preinhaelter, O. Prinz, F. Purps, T. Rajna, S. Récsei, A. Reiman, D. Reiter, J. Remmel, S. Renard, V. Rhode, J. Riemann, S. Rimkevicius, K. Rieße, A. Rodatos, I. Rodin, M. Romé, H.-J. Roscher, K. Rummel, Th. Rummel, A. Runov, L. Ryc, J. Sachtleben, A. Samartsev, M. Sanchez, F. Sano, A. Scarabosio, M. Schmid, H. Schmitz, O. Schmitz, M. Schneider, W. Schneider, L. Scheibl, M. Scholz, G. Schröder, M. Schröder, J. Schruff, H. Schumacher, I.V. Shikhovtsev, M. Shoji, G. Siegl, J. Skodzik, M. Smirnow, E. Speth, D.A. Spong, R. Stadler, Z. Sulek, V. Szabó, T. Szabolics, T. Szetefi, Z. Szökefalvi-Nagy, A. Tereshchenko, H. Thomsen, M. Thumm, D. Timmermann, H. Tittes, K. Toi, M. Tournianski, U.v. Toussaint, J. Tretter, S. Tulipán, P. Turba, R. Uhlemann, J. Urban, E. Urbonavicius, P. Urlings, S. Valet, D. Van Eester, M. Van Schoor, M. Vervier, H. Viebke, R. Vilbrandt, M. Vrancken, T. Wauters, M. Weissgerber, E. Weiß, A. Weller, J. Wendorf, U. Wenzel, T. Windisch, E. Winkler, M. Winkler, J. Wolowski, J. Wolters, G. Wrochna, P. Xanthopoulos, H. Yamada, M. Yokoyama, D. Zacharias, J. Zajac, G. Zangl, M. Zarnstorff, H. Zeplien, S. Zoletnik, and M. Zuin. Technical challenges in the construction of the steady-state stellarator Wendelstein 7-X. *Nuclear Fusion*, 53(12):126001, 2013.

[32] Edward I Moses. Ignition and inertial confinement fusion at the National Ignition Facility. *Journal of Physics: Conference Series*, 244(1):012006, 2010.

[33] J A Wesson. The ohmic heating of a multicomponent plasma. *Journal of Nuclear Energy. Part C, Plasma Physics, Accelerators, Thermonuclear Research*, 4(5):321, 1962.

[34] E Speth. Neutral beam heating of fusion plasmas. *Reports on Progress in Physics*, 52(1):57, 1989.

[35] J Adam. Review of tokamak plasma heating by wave damping in the ion cyclotron range of frequency. *Plasma Physics and Controlled Fusion*, 29(4):443, 1987.

[36] H.F. Dylla. A review of the wall problem and conditioning techniques for tokamaks. *Journal of Nuclear Materials*, 93–94, Part 1(0):61 – 74, 1980.

[37] M Kaufmann. Review on pellet fuelling. *Plasma Physics and Controlled Fusion*, 28(9A):1341, 1986.

[38] P. T. Lang, K. Büchl, M. Kaufmann, R. S. Lang, V. Mertens, H. W. Müller, and J. Neuhauser. High-efficiency plasma refuelling by pellet injection

from the magnetic high-field side into ASDEX Upgrade. *Phys. Rev. Lett.*, 79:1487–1490, Aug 1997.

[39] T. Ihli, T.K. Basu, L.M. Giancarli, S. Konishi, S. Malang, F. Najmabadi, S. Nishio, A.R. Raffray, C.V.S. Rao, A. Sagara, and Y. Wu. Review of blanket designs for advanced fusion reactors. *Fusion Engineering and Design*, 83(7–9):912 – 919, 2008. Proceedings of the Eight International Symposium of Fusion Nuclear Technology ISFNT-8 {SI}.

[40] P.L. Mondino, P. Bayetti, E. Di Pietro, R.S. Hemsworth, H. Iida, T. Inoue, K. Ioki, G. Johnson, A.I. Krylov, V.M. Kulygin, P. Massmann, K. Miyamoto, Y. Okumura, A.A. Panasenkov, R.T. Santoro, M. Sironi, Y. Utin, K. Watanabe, and M. Yamada. ITER neutral beam system. *Nuclear Fusion*, 40(3Y):501, 2000.

[41] K. Tani, K. Shinohara, T. Oikawa, H. Tsutsui, S. Miyamoto, Y. Kusama, and T. Sugie. Effects of ELM mitigation coils on energetic particle confinement in ITER steady-state operation. *Nuclear Fusion*, 52(1):013012, 2012.

[42] Allen H. Boozer. Plasma equilibrium with rational magnetic surfaces. *Physics of Fluids*, 24(11):1999–2003, 1981.

[43] Hannes Risken. Fokker-planck equation. In *The Fokker-Planck Equation*, volume 18 of *Springer Series in Synergetics*, pages 63–95. Springer Berlin Heidelberg, 1984.

[44] A. Salmi, T. Johnson, V. Parail, J. Heikkinen, V. Hynönen, T. P. Kiviniemi, T. Kurki-Suonio, and JET EFDA Contributors. ASCOT modelling of ripple effects on toroidal torque. *Contributions to Plasma Physics*, 48(1-3):77–81, 2008.

[45] V. Hynönen, T. Kurki-Suonio, W. Suttrop, R. Dux, K. Sugiyama, and the ASDEX Upgrade Team. Surface loads and edge fast ion distribution for co- and counter-injection in ASDEX Upgrade. *Plasma Physics and Controlled Fusion*, 49(2):151, 2007.

[46] J. A. Heikkinen and S. K. Sipilä. Power transfer and current generation of fast ions with large-k_θ waves in tokamak plasmas. *Physics of Plasmas*, 2(10):3724–3733, 1995.

[47] T. Kurki-Suonio, O. Asunta, T. Hellsten, V. Hynönen, T. Johnson, T. Koskela, J. Lönnroth, V. Parail, M. Roccella, G. Saibene, A. Salmi, and S. Sipilä. ASCOT simulations of fast ion power loads to the plasma-facing components in ITER. *Nuclear Fusion*, 49(9):095001, 2009.

[48] T. Kurki-Suonio, O. Asunta, E. Hirvijoki, T. Koskela, A. Snicker, T. Hauff, F. Jenko, E. Poli, and S. Sipilä. Fast ion power loads on ITER first wall structures in the presence of NTMs and microturbulence. *Nuclear Fusion*, 51(8):083041, 2011.

[49] A. Snicker, S. Sipilä, and T. Kurki-Suonio. Orbit-following fusion alpha wall load simulation for ITER scenario 4 including full orbit effects. *Nuclear Fusion*, 52(9):094011, 2012.

[50] A. Snicker, E. Hirvijoki, and T. Kurki-Suonio. Power loads to ITER first wall structures due to fusion alphas in a non-axisymmetric magnetic field including the presence of MHD modes. *Nuclear Fusion*, 53(9):093028, 2013.

[51] T. Koskela, O. Asunta, E. Hirvijoki, T. Kurki-Suonio, and S. Äkäslompolo. ITER edge-localized modes control coils: the effect on fast ion losses and edge confinement properties. *Plasma Physics and Controlled Fusion*, 54(10):105008, 2012.

[52] J. Miettunen, T. Kurki-Suonio, T. Makkonen, M. Groth, A. Hakola, E. Hirvijoki, K. Krieger, J. Likonen, S. Äkäslompolo, and the ASDEX Upgrade Team. The effect of non-axisymmetric wall geometry on ^{13}C transport in ASDEX Upgrade. *Nuclear Fusion*, 52(3):032001, 2012.

[53] J. Miettunen, M. Groth, T. Kurki-Suonio, H. Bergsåker, J. Likonen, S. Marsen, C. Silva, and S. Äkäslompolo. Predictive ASCOT modelling of ^{10}Be transport in JET with the ITER-like wall. *Journal of Nuclear Materials*, 438, Supplement(0):S612 – S615, 2013. Proceedings of the 20th International Conference on Plasma-Surface Interactions in Controlled Fusion Devices.

[54] Eero Hirvijoki. *Theory and models for Monte Carlo simulations of minority particle populations in tokamak plasmas*. PhD thesis, Aalto University, School of Science, March 2014.

[55] A. Kolmogorov. Über die analytischen methoden in der wahrscheinlichkeitsrechnung. *Mathematische Annalen*, 104(1):415–458, 1931.

[56] E. Hirvijoki, A. Brizard, A. Snicker, and T. Kurki-Suonio. Monte Carlo implementation of a guiding-center fokker-planck kinetic equation. *Physics of Plasmas*, 20(9):092505, 2013.

[57] NTCC PSPLINE Module. http://w3.pppl.gov/ntcc/PSPLINE/.

[58] D. Badouel. *An Efficient Ray-Polygon Intersection*, pages 390–393. Graphics Gems. Academic Press, 1990.

[59] HELIOS supercomputer. http://www.iferc.org/csc/csc_for_researchers/csc_introduction.html.

[60] CSC - IT centre for science. http://www.csc.fi/english.

[61] The HDF Group. Hierarchical data format version 5. http://www.hdfgroup.org/HDF5, 2000-2010.

[62] O. Asunta, J. Govenius, R. Budny, M. Gorelenkova, G. Tardini, T. Kurki-Suonio, A. Salmi, S. Sipilä, the ASDEX Upgrade Team, and the JET EFDA Contributors. Modelling neutral beams in fusion devices: Beamlet-based model for fast particle simulations. *accepted for publication in Computer Physics Communications*, 2014.

[63] H. Mimata, K. Tani, K. Tobita, H. Tsutsui, S. Tsuji-Iio, and R. Shimada. Finite larmor radius effects on ripple diffusion in tokamaks. *Progress in Nuclear Energy*, 50(2-6):638 – 642, 2008. Innovative Nuclear Energy Systems for Sustainable Development of the World. Proceedings of the Second COE-INES International Symposium, INES-2, November 26-30, 2006, Yokohama, Japan.

[64] O. Asunta, S. Äkäslompolo, T. Kurki-Suonio, T. Koskela, S. Sipilä, A. Snicker, M. Garcia-Muńoz, and the ASDEX Upgrade team. Simulations of fast ion wall loads in ASDEX Upgrade in the presence of magnetic perturbations due to ELM-mitigation coils. *Nuclear Fusion*, 52(9):094014, 2012.

[65] H. X. Vu and J. U. Brackbill. Accurate numerical solution of charged particle motion in a magnetic field. *Journal of Computational Physics*, 116(2):384 – 387, 1995.

[66] M. García-Muñoz, P. Martin, H.-U. Fahrbach, M. Gobbin, S. Günter, M. Maraschek, L. Marrelli, H. Zohm, and the ASDEX Upgrade Team. NTM induced fast ion losses in ASDEX Upgrade. *Nuclear Fusion*, 47(7):L10–L15, July 2007.

[67] M. García-Muñoz, H.-U. Fahrbach, S. Gunter, V. Igochine, M. J. Mantsinen, M. Maraschek, P. Martin, P. Piovesan, K. Sassenberg, and H. Zohm. Fast-Ion Losses due to High-Frequency MHD Perturbations in the ASDEX Upgrade Tokamak. *Physical Review Letters*, 100(5):055005, 2008.

[68] M.A. Van Zeeland, N.N. Gorelenkov, W.W. Heidbrink, G.J. Kramer, D.A. Spong, M.E. Austin, R.K. Fisher, M. García Muñoz, M. Gorelenkova, N. Luhmann, M. Murakami, R. Nazikian, D.C. Pace, J.M. Park, B.J. Tobias, and R.B. White. Alfvén eigenmode stability and fast ion loss in DIII-D and ITER reversed magnetic shear plasmas. *Nuclear Fusion*, 52(9):094023, 2012.

[69] W. W. Heidbrink, E. J. Strait, M. S. Chu, and A. D. Turnbull. Observation of beta-induced Alfvén eigenmodes in the DIII-D tokamak. *Phys. Rev. Lett.*, 71:855–858, Aug 1993.

[70] X. Chen, M. E. Austin, R. K. Fisher, W. W. Heidbrink, G. J. Kramer, R. Nazikian, D. C. Pace, C. C. Petty, and M. A. Van Zeeland. Enhanced localized energetic-ion losses resulting from single-pass interactions with Alfvén Eigenmodes. *Phys. Rev. Lett.*, 110:065004, Feb 2013.

[71] K. L. Wong, R. J. Fonck, S. F. Paul, D. R. Roberts, E. D. Fredrickson, R. Nazikian, H. K. Park, M. Bell, N. L. Bretz, R. Budny, S. Cohen, G. W. Hammett, F. C. Jobes, D. M. Meade, S. S. Medley, D. Mueller, Y. Nagayama, D. K. Owens, and E. J. Synakowski. Excitation of toroidal Alfvén eigenmodes in TFTR. *Phys. Rev. Lett.*, 66:1874–1877, Apr 1991.

[72] Q. Yu. Numerical modeling of diffusive heat transport across magnetic islands and local stochastic field. *Physics of Plasmas*, 13(6):062310, 2006.

[73] E. Strumberger, S. Günter, E. Schwarz, C. Tichmann, and the ASDEX Upgrade Team. Fast particle losses due to NTMs and magnetic field ripple. *New Journal of Physics*, 10(2):023017 (21pp), 2008.

[74] A.A. Galeev and R.Z. Sagdeev. Transport phenomena in a collisionless plasma in a toroidal magnetic system. *Sov. Phys. JETP*, 26(1):233, 1968.

[75] A.A. Galeev. Diffusion-electrical phenomena in a plasma confined in a tokamak machine. *Sov. Phys. JETP*, 32(4):752, 1971.

[76] A.A. Galeev and R.Z. Sagdeev. *JETP letts*, 13:113, 1971.

[77] R.Z. Sagdeev and A.A. Galeev. *Sov. Phys. Dokl.*, 14:1198, 1970.

[78] R. J. Bickerton, J. W. Connor, and J.B. Tayloret. Diffusion driven plasma currents and bootstrap tokamak. *Nature (Phys. Sci.)*, 229:110–112, Jan 1971.

[79] M Kikuchi. Prospects of a stationary tokamak reactor. *Plasma Physics and Controlled Fusion*, 35(SB):B39, 1993.

[80] M. Schneider, L.-G. Eriksson, V Basiuk, and F Imbeaux. On alpha particle effects in tokamaks with a current hole. *Plasma Physics and Controlled Fusion*, 47(12):2087, 2005.

[81] H. Biglari, P. H. Diamond, and P. W. Terry. Influence of sheared poloidal rotation on edge turbulence. *Physics of Fluids B: Plasma Physics (1989-1993)*, 2(1):1–4, 1990.

[82] P. W. Terry. Suppression of turbulence and transport by sheared flow. *Rev. Mod. Phys.*, 72:109–165, Jan 2000.

[83] A. Bondeson and D. J. Ward. Stabilization of external modes in tokamaks by resistive walls and plasma rotation. *Phys. Rev. Lett.*, 72:2709–2712, Apr 1994.

[84] M. Bécoulet, G. Huysmans, X. Garbet, E. Nardon, D. Howell, A. Garofalo, M. Schaffer, T. Evans, K. Shaing, A. Cole, J.-K. Park, and P. Cahyna. Physics of penetration of resonant magnetic perturbations used for Type I edge localized modes suppression in tokamaks. *Nuclear Fusion*, 49(8):085011, 2009.

[85] M.N. Rosenbluth and F.L. Hinton. Plasma rotation driven by alpha particles in a tokamak reactor. *Nuclear Fusion*, 36(1):55, 1996.

[86] K Tani and M Azumi. Simulation studies on alpha-particle-driven current in tokamak reactors. *Nuclear Fusion*, 48(8):085001, 2008.

[87] M. Honda, T. Takizuka, K. Tobita, G. Matsunaga, and A. Fukuyama. Alpha particle-driven toroidal rotation in burning plasmas. *Nuclear Fusion*, 51(7):073018, 2011.

[88] M. García-Muñoz, H.-U. Fahrbach, H. Zohm, and the ASDEX Upgrade Team. Scintillator based detector for fast-ion losses induced by magnetohydrodynamic instabilities in the ASDEX upgrade tokamak. *Review of Scientific Instruments*, 80(5):053503, 2009.

[89] M. Garcia-Munoz, I.G.J. Classen, B. Geiger, W.W. Heidbrink, M.A. Van Zeeland, S. Äkäslompolo, R. Bilato, V. Bobkov, M. Brambilla, G.D. Conway, S. da Graça, V. Igochine, Ph. Lauber, N. Luhmann, M. Maraschek, F. Meo, H. Park, M. Schneller, G. Tardini, and the ASDEX Upgrade Team. Fast-ion transport induced by Alfvén eigenmodes in the ASDEX Upgrade tokamak. *Nuclear Fusion*, 51(10):103013, 2011.

[90] R.B. White. *The theory of toroidally confined systems*. Imperial college Press, 2nd edition, 2001.

[91] B Geiger, M Garcia-Munoz, W W Heidbrink, R M McDermott, G Tardini, R Dux, R Fischer, V Igochine, and the ASDEX Upgrade Team. Fast-ion D-alpha measurements at ASDEX Upgrade. *Plasma Physics and Controlled Fusion*, 53(6):065010, 2011.

[92] M. Salewski, F. Meo, M. Stejner, O. Asunta, H. Bindslev, V. Furtula, S.B. Korsholm, T. Kurki-Suonio, F. Leipold, F. Leuterer, P.K. Michelsen, D. Moseev, S.K. Nielsen, J. Stober, G. Tardini, D. Wagner, P. Woskov, and the ASDEX Upgrade team. Comparison of fast ion collective thomson scattering measurements at ASDEX upgrade with numerical simulations. *Nuclear Fusion*, 50(3):035012, 2010.

[93] M. Salewski, B. Geiger, S.K. Nielsen, H. Bindslev, M. García-Muñoz, W.W. Heidbrink, S.B. Korsholm, F. Leipold, J. Madsen, F. Meo, P.K. Michelsen, D. Moseev, M. Stejner, G. Tardini, and the ASDEX Upgrade Team. Combination of fast-ion diagnostics in velocity-space tomographies. *Nuclear Fusion*, 53(6):063019, 2013.

[94] M. Salewski, B. Geiger, A.S. Jacobsen, M. García-Muñoz, W.W. Heidbrink, S.B. Korsholm, F. Leipold, J. Madsen, D. Moseev, S.K. Nielsen, J. Rasmussen, M. Stejner, G. Tardini, M. Weiland, and the ASDEX Upgrade Team. Measurement of a 2D fast-ion velocity distribution function by tomographic inversion of fast-ion D-alpha spectra. *Nuclear Fusion*, 54(2):023005, 2014.

[95] S.D. Pinches, V.G. Kiptily, S.E. Sharapov, D.S. Darrow, L.-G. Eriksson, H.-U. Fahrbach, M. García-Muñoz, M. Reich, E. Strumberger, A. Werner, the ASDEX Upgrade Team, and JET-EFDA Contributors. Observation and modelling of fast ion loss in JET and ASDEX Upgrade. *Nuclear Fusion*, 46(10):S904–S910, October 2006.

[96] N N Gorelenkov and R B White. Perturbative study of energetic particle redistribution by Alfvén eigenmodes in ITER. *Plasma Physics and Controlled Fusion*, 55(1):015007, 2013.

[97] G.J. Kramer, B.V. Budny, R. Ellis, M. Gorelenkova, W.W. Heidbrink, T. Kurki-Suonio, R. Nazikian, A. Salmi, M.J. Schaffer, K. Shinohara, J.A. Snipes, D.A. Spong, T. Koskela, and M.A. Van Zeeland. Fast-ion effects during test blanket module simulation experiments in DIII-D. *Nuclear Fusion*, 51(10):103029, 2011.

[98] K. Shinohara, T. Kurki-Suonio, D. Spong, O. Asunta, K. Tani, E. Strumberger, S. Briguglio, T. Koskela, G. Vlad, S. Günter, G. Kramer, S. Putvinski, K. Hamamatsu, and ITPA Topical Group on Energetic Particles. Effects of complex symmetry-breakings on alpha particle power loads on first wall structures and equilibrium in ITER. *Nuclear Fusion*, 51(6):063028, 2011.

[99] H. van den Brand, M. R. de Baar, N. J. Lopes Cardozo, and E. Westerhof. Integrated modelling of island growth, stabilization and mode locking: consequences for NTM control on ITER. *Plasma Physics and Controlled Fusion*, 54(9):094003, 2012.

[100] R.J. La Haye, R. Prater, R.J. Buttery, N. Hayashi, A. Isayama, M.E. Maraschek, L. Urso, and H. Zohm. Cross-machine benchmarking for ITER

of neoclassical tearing mode stabilization by electron cyclotron current drive. *Nuclear Fusion*, 46(4):451, 2006.

[101] T. Hirai, K. Ezato, and P. Majerus. ITER relevant high heat flux testing on plasma facing components. *Materials Transactions*, 46(3):412–424, 2005.

[102] Ph. Lauber, S. Günter, A. Könies, and S.D. Pinches. LIGKA: A linear gyrokinetic code for the description of background kinetic and fast particle effects on the MHD stability in tokamaks. *Journal of Computational Physics*, 226(1):447 – 465, 2007.

[103] R. Hawryluk. An empirical approach to tokamak transport. In B. Coppi, G.G. Leotta, D. Pfirsch, R. Pozzoli, and E. Sindoni, editors, *Physics of Plasmas Close to Thermonuclear Conditions, Volume 1*, volume 1, pages 19–46, Oxford, UK, 1981. Pergamon Press.

[104] A. Pankin, D. McCune, R. Andre, G. Bateman, and A. Kritz. The tokamak Monte Carlo fast ion module NUBEAM in the national transport code collaboration library. *Computer Physics Communications*, 159(3):157 – 184, 2004.

[105] WW Heidbrink, D Liu, Y Luo, E Ruskov, and B Geiger. A code that simulates fast-ion D-alpha and neutral particle measurements. *Comm. Comp. Physics*, 8, 2010.

[106] K G McClements and A Thyagaraja. Collisionless fast particle transport in tokamak plasmas with rotating magnetic islands. *Plasma Physics and Controlled Fusion*, 49(9):1415, 2007.

[107] E. Poli, A. Bergmann, A.G. Peeters, L.C. Appel, and S.D. Pinches. Kinetic calculation of the polarization current in the presence of a neoclassical tearing mode. *Nuclear Fusion*, 45(5):384, 2005.

Aalto-DD 199/2014

ISBN 978-952-60-5993-8 (printed)
ISBN 978-952-60-5994-5 (pdf)
ISSN-L 1799-4934
ISSN 1799-4934 (printed)
ISSN 1799-4942 (pdf)

Aalto University
School of Science
Department of Applied Physics
www.aalto.fi

BUSINESS + ECONOMY

ART + DESIGN + ARCHITECTURE

SCIENCE + TECHNOLOGY

CROSSOVER

DOCTORAL DISSERTATIONS